SACLANTCEN MEMORANDUM
serial no.: SM-290

SACLANT UNDERSEA
RESEARCH CENTRE

MEMORANDUM

Benchmarking scattering in ocean waveguides

F.B. Jensen, C.M. Ferla
and P. Gerstoft

July 1995

Page count for SM-290 (excluding Covers and Data Sheet)

Pages	Total
i–vi	6
1–58	58
	64

SACLANT Undersea Research Centre
Viale San Bartolomeo 400
19138 San Bartolomeo (SP), Italy

tel: +39-187-540.111
fax: +39-187-524.600

e-mail: library@saclantc.nato.int

NORTH ATLANTIC TREATY ORGANIZATION

SACLANTCEN SM-290

Benchmarking scattering in ocean waveguides

F.B. Jensen, C.M. Ferla and P. Gerstoft

The content of this document pertains to work performed under Project 19 of the SACLANTCEN Programme of Work. The document has been approved for release by The Director, SACLANTCEN.

Issued by:
Environmental Research Division

W.I. Roderick
Division Chief

intentionally blank page

Benchmarking scattering in ocean waveguides

F.B. Jensen, C.M. Ferla and P. Gerstoft

Executive Summary: Acoustic models play a central role in the analysis and interpretation of propagation, reverberation, and noise data as well as for the assessment of sonar performance in complex ocean environments. The validation of general-purpose numerical models, however, poses a problem because of the lack of known (analytic) reference solutions for realistic ocean-acoustic scenarios. Earlier attempts to provide numerical reference solutions for *propagation* in canonical ocean environments were quite successful, but, so far, little effort has gone into establishing similar reference solutions for *scattering*.

In recognition of this fact, a Reverberation and Scattering Workshop was convened in Gulfport, MS, on May 2–6, 1994. A set of test problems involving forward scattering from a rough sea surface as well as backscattering from obstacles on the seafloor were defined, and the modeling community was invited to try to generate accurate solutions with different numerical codes. It was hoped, of course, that such an exercise would lead to a consensus solution, i.e., an accepted reference solution for the posed benchmark problems.

This report presents the SACLANTCEN contributions towards establishing benchmark solutions for simple scattering and reverberation problems in the ocean. We obtained numerically stable solutions for all test problems (CW and broadband) with the codes that in the past were used successfully to provide reference solutions to other benchmark problems in ocean acoustics. Hence, we are confident that also the numerical results presented here for the scattering problems are accurate solutions that can serve as references for future model validations.

intentionally blank page

Report no. changed (Mar 2006): SM-290-UU

SACLANTCEN SM-290

Benchmarking scattering in ocean waveguides

F.B. Jensen, C.M. Ferla and P. Gerstoft

Abstract: Accurate numerical solutions are presented for benchmark problems associated with forward scattering from a rough sea surface and with backscattering from obstacles on the seafloor in a shallow-water waveguide. Computational aspects are discussed and both CW (transmission loss at 30 Hz) and broadband (10–50 Hz) time-series solutions are given.

Keywords: numerical modeling ○ propagation loss ○ pulse modeling ○ reverberation ○ scattering

Contents

1
Introduction

Reference solutions to simple acoustic problems serve the purpose of providing benchmarks for complex numerical codes, whose overall performance can be assessed only by comparison with known reference solutions. This, however, is a typical Catch 22 situation, since 'reference' solutions to realistic ocean-acoustic problems can be obtained only from *numerical* solutions of the wave equation. Hence the approach has been to exercise different numerical solution schemes (rays, modes, spectral techniques, parabolic equations, etc. [1]) on a set of benchmark problems to try to obtain consistent solutions which could be considered a reference for further model testing. Such an exercise was successfully undertaken within the Acoustical Society of America a few years ago for the forward scattered field in a simple wedge geometry [2], and, more recently, additional test problems very solved as part of the PE Workshop II [3].

Up till now, attempts to provide a reference solution for the backscattered field in a waveguide have been sparse [4], and that, exactly, was the reason why the Reverberation and Scattering Workshop was convened in Gulfport, MS, on May 2–6, 1994 [5]. As shown in Annex A, five test problems were proposed and solved: one dealing with forward scattering from a rough sea surface, and four with backscattering from obstacles on the seafloor. An additional test problem dealing with the modeling of real scattering data collected along the Mid-Atlantic Ridge was not solved by us.

Table 1 contains pertinent information on parameter selections and CPU times for the different numerical codes used to solve the five test problems. From left to right, the table lists the test cases, whether it is a continuous wave (CW) or a broadband (BB) calculation, followed by the name of the acoustic model used. The next three columns give numerical input parameters mainly related to the COUPLE normal-mode code [6,7]. H_{B} is the false bottom depth, while H_{A} is the depth where the deep attenuation layer starts. Next is given the number of modes (`NM`) included in the calculation, followed by the number of range segments (`NSEG`) used to describe the bottom topography. The column indicated by `NF` is the number of frequencies for a broadband calculation. Finally, the last column gives the CPU time on a DEC 3000/400 workstation. The CPU time increases linearly with the number of frequencies (`NF`) and the number of range segments (`NSEG`), but quadraticly with the number of modes (`NM`). We shall be referring back to this summary table while discussing each test case in detail.

Whereas Case 1 (forward scattering from a rough sea surface) was solved by one of the standard PE codes [8,9], the remaining test problems associated with back-

Table 1 *Numerical parameters and CPU times on DEC 3000/400*

Test		Model	H_B/H_A (m)	NM	NSEG	NF	CPU
Case 1:	CW	IFD	$\Delta r = 0.375$ m $\Delta z = 0.250$ m	–	–	–	< 1 min
Case 2a:	CW	COUPLE	1000/500	50	3	1	< 1 min
	BB		500/300	25	3	320	15 min
Case 2b:	CW	COUPLE	1000/500	50	103	1	10 min
	BB		500/300	25	23	320	1.5 h
Case 3a:	CW	COUPLE	1000/500	50	5	1	< 1 min
	BB		500/300	25	5	320	30 min
Case 3b:	CW	COUPLE	1000/500	70	205	1	30 min
	BB		500/300	25	45	320	3 h
Case 4:	CW	COUPLE	1000/500	50	5	1	< 1 min
	BB		650/450	30	5	320	30 min
Case 5a,b:	CW	COUPLE	1000/500	100	22	1	10 min
	BB		500/300	40	22	320	4 h
Case 5c,d:	CW	COUPLE	1000/500	100	22	1	10 min
	BB		500/300	40	22	1280	16 h

scattering from obstacles of different shapes on the seafloor, were all solved by the stepwise coupled normal-mode code (COUPLE) developed by Evans more than a decade ago [6] and recently upgraded to include a deep attenuation layer in the bottom [7]. We originally solved these problems with the old code (no absorption layer) which required a false bottom depth of 3000 m and the computation of 150–300 modes to get a full-spectrum, noise-free solution. Not only were the CPU times exorbitant, but various numerical overflow problems precluded running full convergence tests in several cases.

The new version of COUPLE presented at the R&S Workshop turned out to have such an improved performance (20–50 times speed-up) that it was immediately selected as our benchmark code. The improved performance was achieved by introducing an absorption layer with a linearly increasing attenuation deep in the bottom. (This is the 'sponge' layer approach used also in PE's [1] to avoid reflections off the lower computational boundary – the false bottom.) As seen in Table 1, the new COUPLE code provides numerically stable, noise-free CW solutions with a false bottom depth of $H_B = 1000$ m and an absorption layer starting at $H_A = 500$ m, with the attenuation increasing linearly from 0.5 dB/λ at the top of the layer (500 m) to 5.0 dB/λ at the bottom (1000 m). Since the number of modes required to get a full-spectrum solution is proportional to the false bottom depth H_B, we can now do the problems by computing just 50–100 modes. We also see from Table 1 that the

broadband problems were done with a false bottom depth of just 500 m and half the number of modes (see Subsect. 7.1 for details).

This report is structured as a self-consistent main text containing a short description of each test problem and its solution, plus a few illustrative numerical results. Annex A gives a detailed description of the five test cases in exactly the form provided by the organizers of the R&S Workshop. Annex B, on the other hand, presents full-page numerical solutions of all test problems for easy comparison with other solutions.

2
Case 1

We here consider *forward* scattering from a rough sea surface bounding a homogeneous water halfspace (Annex A). At a first glance this test problem may not seem solvable by standard acoustic models, since they are all set up to treat a flat pressure-release (water–vacuum) sea surface. However, Thomson [10] showed that by adding an air layer on top and treating the rough sea surface as an internal layer boundary between two acoustic media (air and water) we obtain a problem that is easily solved by standard numerical codes.

We start by solving the flat-surface problem shown in Fig. 1. The air layer is 20-m thick with a sound speed of 340 m/s and a density of 0.0012 g/cm^3. The water halfspace has a speed of 1500 m/s and a density of 1.0 g/cm^3. The source field is a 400-Hz Gaussian beam tilted towards the surface. The nominal beam tilt is $-10°$ with the beam center intersecting the surface at mid-range (375 m).

The solution for the flat-surface problem shown in Fig. 1 was generated by the wide-angled version of the IFD PE code developed by Lee *et al.* more than a decade ago [8,9]. Numerically stable results were obtained with a computational grid of $\Delta r = 0.375$ m and $\Delta z = 0.25$ m in less than 1 min on a DEC 3000/400 workstation (Table 1). The solution looks clean, but there is actually energy being transmitted through the water–air interface. To avoid having the solution in the water contaminated by sound propagating in the air layer, we introduced an attenuation in the air of 1 dB/λ.

The rough sea surface was provided as a height profile containing 2000 discrete surface values over the range of 750 m, i.e., a range sampling consistent with the chosen computational grid size of $\Delta r = 0.375$ m. The peak surface excursion is of the order of a wavelength ($\lambda = 3.75$ m), and, hence, we are here dealing with quite a rough sea surface. The IFD solution for the scattered beam is given in Fig. 2; numerically stable results were obtained with the same parameters as given for the flat sea surface. Note that the primary effect of the rough surface is a transfer of energy into steeper propagation angles.

A comparison of the IFD solution versus depth at 750 m with the reference solution (also numerically generated!) of Thorsos [11] show excellent agreement, particularly in the upper 150 m (Fig. 3). Below this depth the angular limitation of the PE (Claerbout form [1]) causes a slight shift in the interference pattern. Clearly, better agreement could be achieved by simply using a higher-angle PE. The IFD solution in Fig. 3 was slightly contaminated by numerical noise, and the curve shown has

been smoothed by a 5-point (1.25 m) running window. It is not clear what causes the numerical noise in the IFD solution, but various tests with a thicker air layer and more attenuation in the layer did not improve the result. (Note that full-page test problem solutions are available in Annex B.)

In conclusion, wide-angle PE codes are well suited for studying forward scattering problems in ocean waveguides.

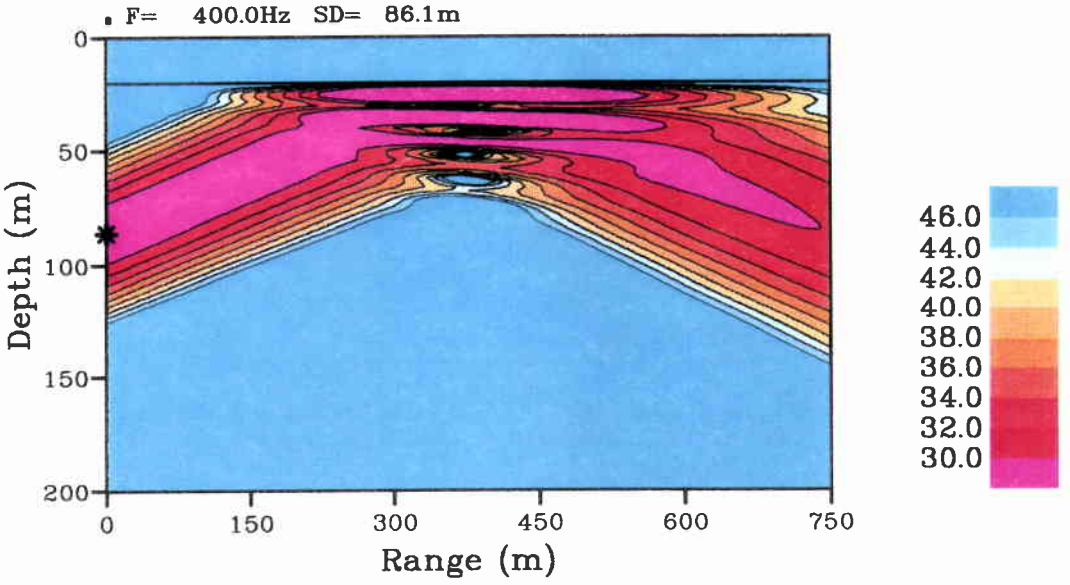

Figure 1 *Case 1:* IFD *solution for Gaussian beam reflected at a flat sea surface.*

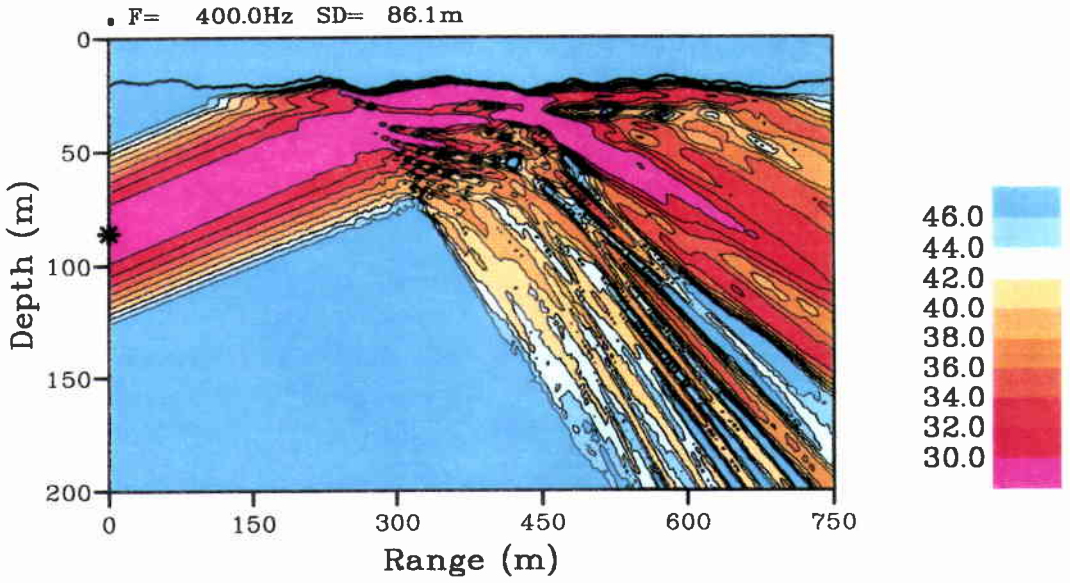

Figure 2 *Case 1:* IFD *solution for Gaussian beam scattered at a rough sea surface.*

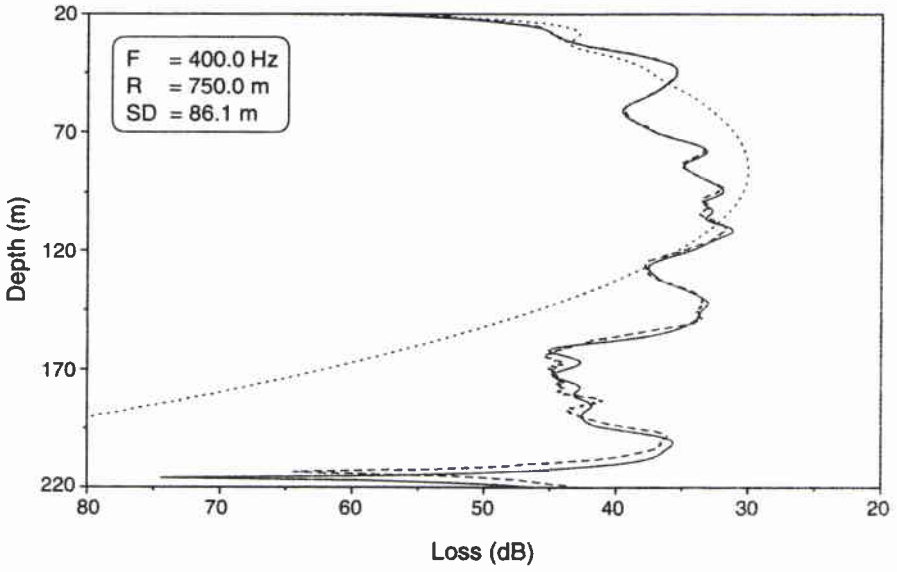

Figure 3 *Case 1: Comparison of* IFD *result (dashed line) with reference solution (solid line) for the forward scattered field vs. depth. The dotted line is the* IFD *result for a flat sea surface.*

3
Case 2

This and the following three test problems all deal with backscattering in shallow-water waveguides due to obstacles of different shapes on the seafloor, see Annex A. As shown in Fig. 4, Case 2a has a single obstacle of height 100 m and thickness 120 m placed 3 km downrange. The obstacle has the same acoustic properties as the seafloor, i.e., a sound speed of 1800 m/s, a density of 1.5 g/cm^3, and an attenuation of 0.5 dB/λ. The water column is homogeneous with a speed of 1500 m/s, a density of 1.0 g/cm^3, and no attenuation. We consider a 30-Hz source placed at 50-m depth, and we solve for both the backscattered and the total field in the waveguide assuming a plane geometry problem (line source).

Case 2b differs from 2a only in the rounding of the top of the obstacle with a radius of curvature of 60 m. Hence Case 2b becomes a test of the stairstep approximation used to represent a semi-circular obstacle shape.

Since no reference solutions were available for these test problems, we started off by comparing the COUPLE results with those obtained from a boundary-element code (BEM) developed by Gerstoft and Schmidt [12]. This code handles scattering from an elastic enclosure in an otherwise horizontally stratified fluid–elastic waveguide. The solution approach is based on Green's theorem which relates the fields in the exterior and interior domains via a boundary integral along the surface of the enclosure. The field solution in the waveguide (exterior domain) is expressed in terms of a wavenumber integral and solved efficiently by the SAFARI code. The scattered field from the enclosure is determined by a discretization of the boundary integral along the surface of the enclosure. The computational effort is considerable, at least two orders of magnitude slower than COUPLE for these types of problems.

Since both COUPLE and BEM are full wave models that include diffraction as well as multiple-scattering effects, both codes should provide accurate solutions to these waveguide problems, assuming, of course, that both codes are pushed to full numerical convergence. The computed backscattered fields from COUPLE and BEM are compared in Figs. 5 and 6 for Cases 2a and 2b, respectively. Note that there were some problems in obtaining full numerical convergence for the BEM code for Case 2b, which explains the small differences observed in Fig. 6. All in all, the agreement between the solutions generated by these two distinctly different numerical codes is so close, that we are confident that the COUPLE solutions presented here and in the following examples are accurate to within a fraction of a decibel.

The COUPLE results for Cases 2a and 2b are given in Figs. 7 and 8. Note that

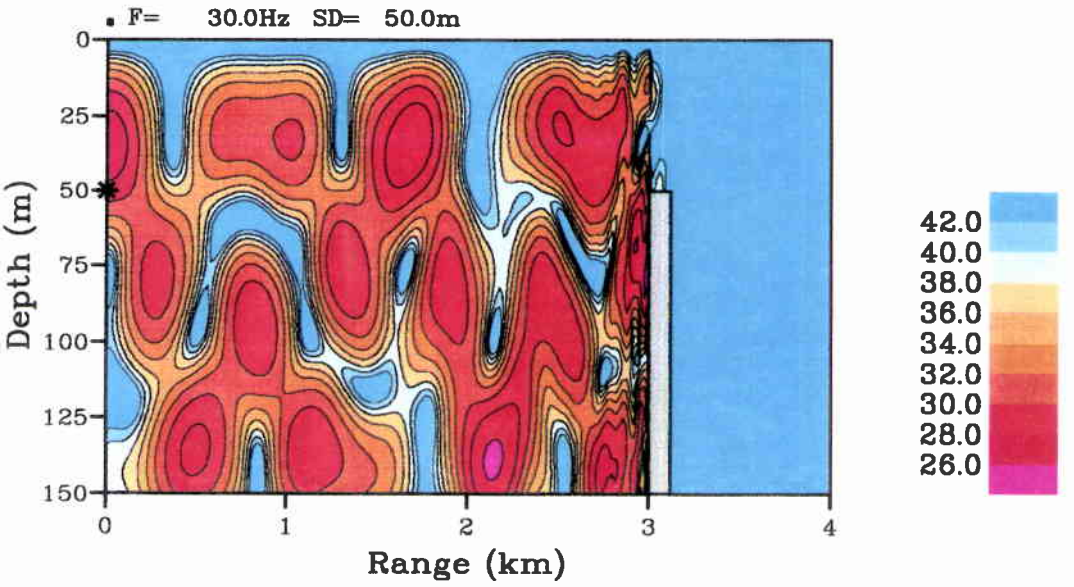

Figure 4 *Case 2a: Computed backscattered field from obstacle placed 3 km downrange.*

the backscattered level is about 10 dB lower for the rounded-top obstacle (Case 2b) compared to the flat-top obstacle (Case 2a). The 'noisy' structure of the total solution (solid line) is interference between the outgoing and backscattered field components. The noise is seen to be absent beyond 3.12 km, where the field is entirely outgoing.

Numerically stable results for Case 2 were obtained with the parameters given in Table 1, i.e., using 50 modes and 101 stairsteps (with equidistant horizontal spacing) across the rounded obstacle in Case 2b.

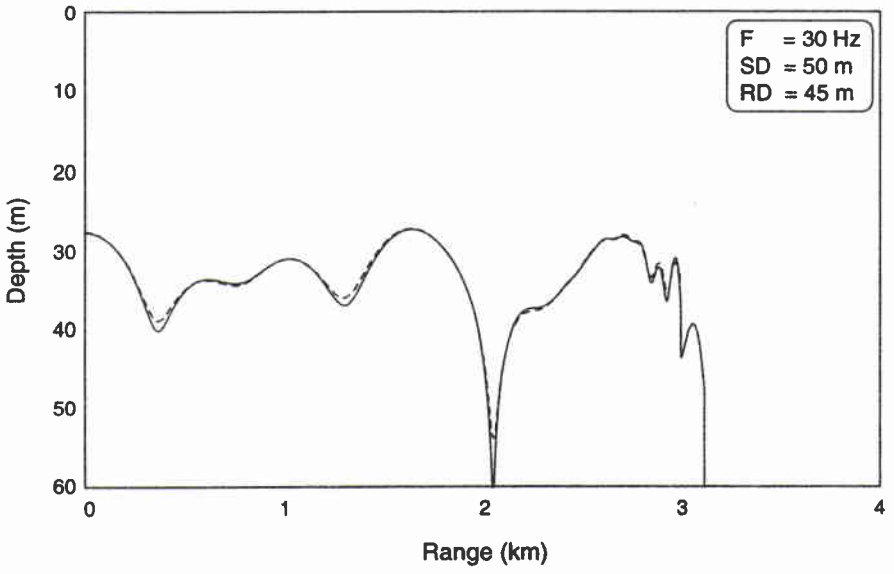

Figure 5 *Case 2a: Comparison of* COUPLE *(solid line) and* BEM *(dashed line) solutions for the backscattered field.*

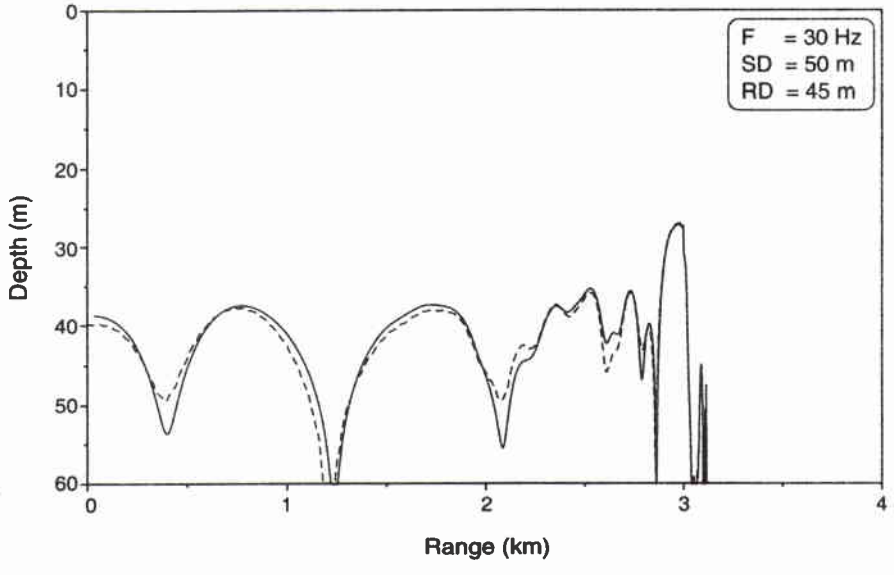

Figure 6 *Case 2b: Comparison of* COUPLE *(solid line) and* BEM *(dashed line) solutions for the backscattered field.*

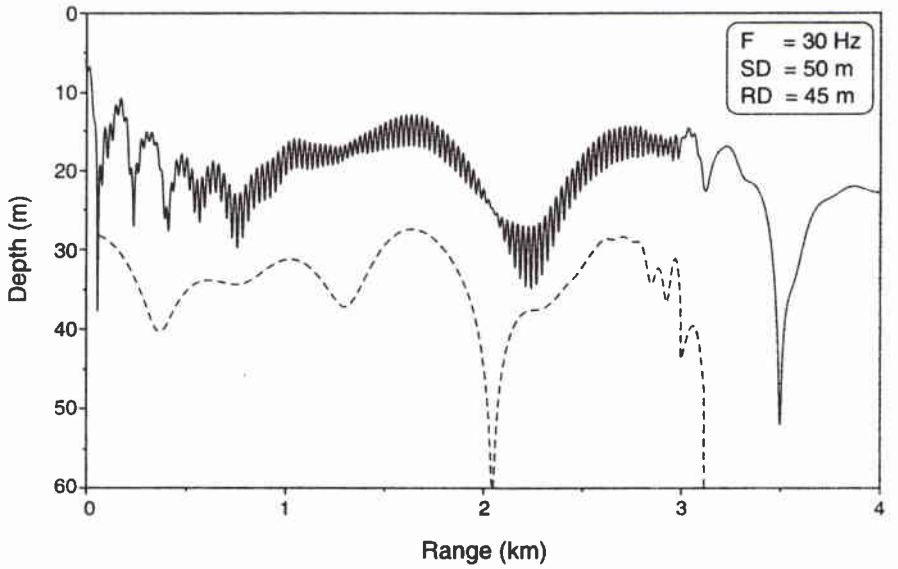

Figure 7 *Case 2a:* COUPLE *solutions for the total field (solid line) as well as the backscattered field component (dashed line).*

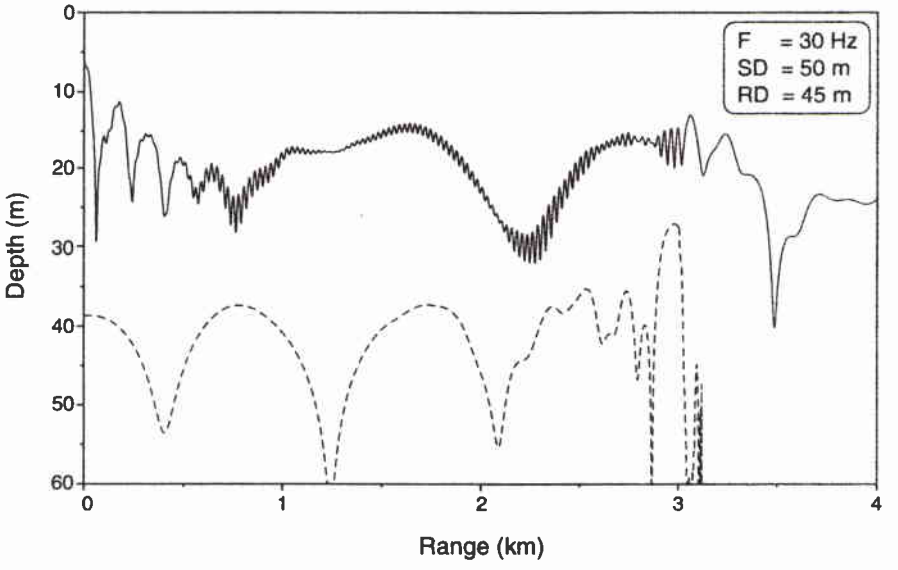

Figure 8 *Case 2b:* COUPLE *solutions for the total field (solid line) as well as the backscattered field component (dashed line).*

4

Case 3

As shown in Annex A, we here consider scattering from two obstacles placed 100 m apart, but each with the same dimensions and acoustic properties as in Case 2 (Fig. 9). Case 3a is for two flat-top obstacles, whereas Case 3b is for two rounded-top obstacles. The added complication here is that this test problem involves multiple scattering between the two obstacles. Again, we solve for both the backscattered and the total field in the waveguide assuming a plane geometry problem (line source).

The COUPLE results for Cases 3a and 3b are given in Figs. 10 and 11, respectively. We again see that the backscattered level generally is 10 dB lower for the rounded-top obstacles (Case 3b) compared to the flat-top obstacles (Case 3a). However, the backscattered field in Fig. 11 is very strong right above the two rounded obstacles ($\sim$ 3 km) indicating that considerable energy is being scattered into steep propagation angles. This clearly has implications for the numerical convergence, since an accurate representation of steeper angle energy requires more modes in the calculation. In fact, as seen from Table 1, numerically stable results for Case 3b required 70 modes (vs. 50 modes for Case 3a) and 101 stairsteps per obstacle.

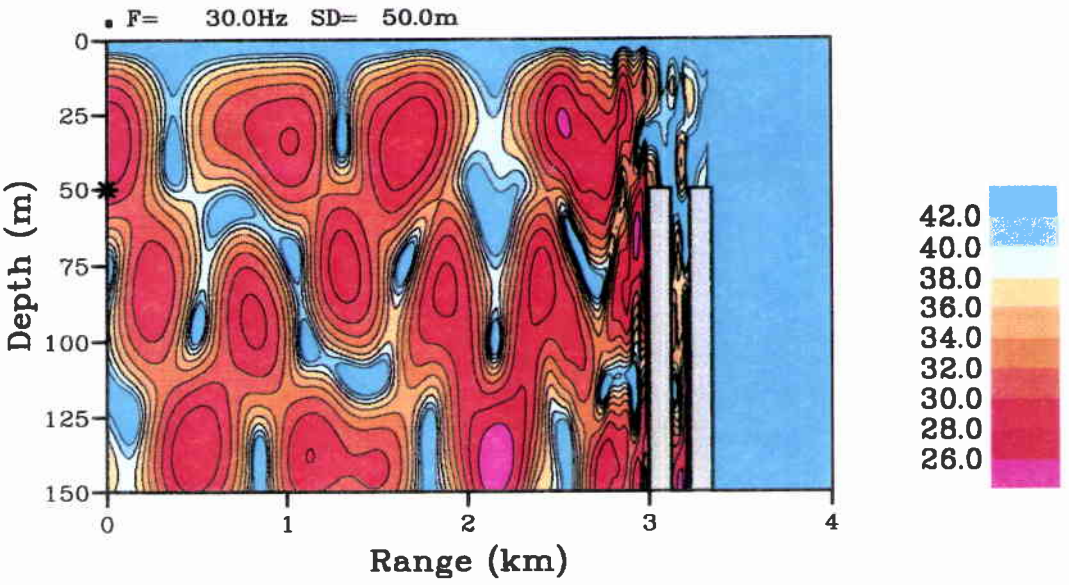

Figure 9 *Case 3a: Computed backscattered field from two obstacles placed 3 km down-range.*

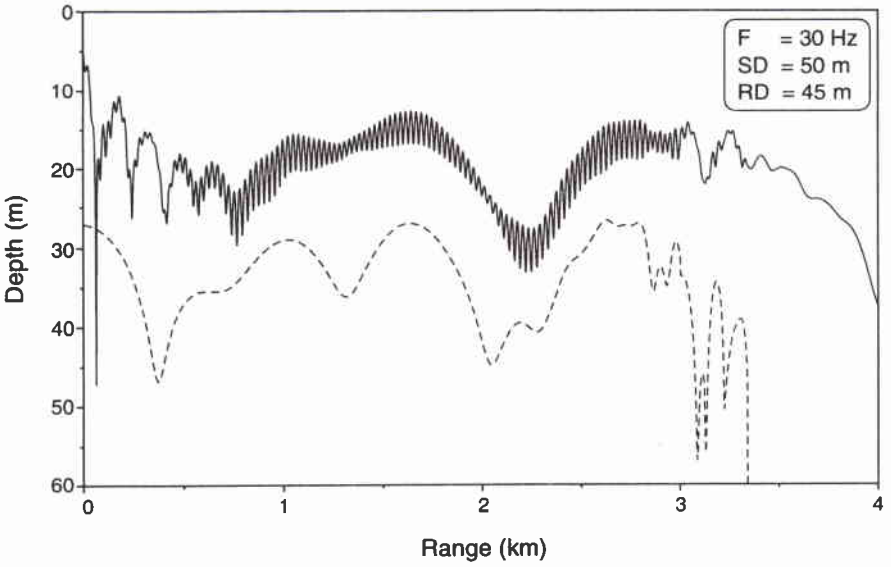

Figure 10 *Case 3a:* COUPLE *solutions for the total field (solid line) as well as the backscattered field component (dashed line).*

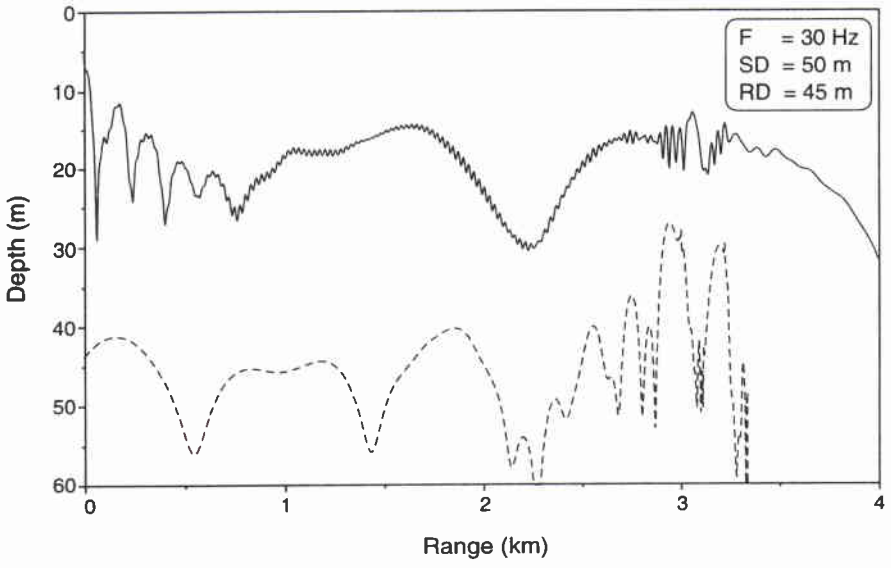

Figure 11 *Case 3b:* COUPLE *solutions for the total field (solid line) as well as the backscattered field component (dashed line).*

5 Case 4

It is not just protruding obstacles on the seafloor that cause backscattering; any deviation from a flat, smooth seafloor gives rise to a back-propagated field. As shown in Fig. 12 and in Annex A, we here consider 'holes' or troughs in the bottom, again placed 3 km downrange. The water-filled holes are 100-m deep and have flat bottoms. Two cases are considered: (i) two holes of width 100 m spaced 120 m apart, with receivers at 45 m (Case 4a) and 125 m (Case 4b), and (ii) two holes of width 60 m spaced 120 m apart, with receivers at 45 m (Case 4c) and 125 m (Case 4d). Again, we solve for both the backscattered and the total field in the waveguide assuming a plane geometry problem (line source).

These test problems did not present particular computational problems, and numerically stable solutions were achieved in all cases by using 50 modes (Table 1). As expected, the backscattered level is here much lower than when considering protruding obstacles. Thus, for Case 4a (Fig. 13) the backscattered field is nearly 30 dB lower than the outgoing field. Solutions for all Case-4 problems are given as full-page figures in Annex B.

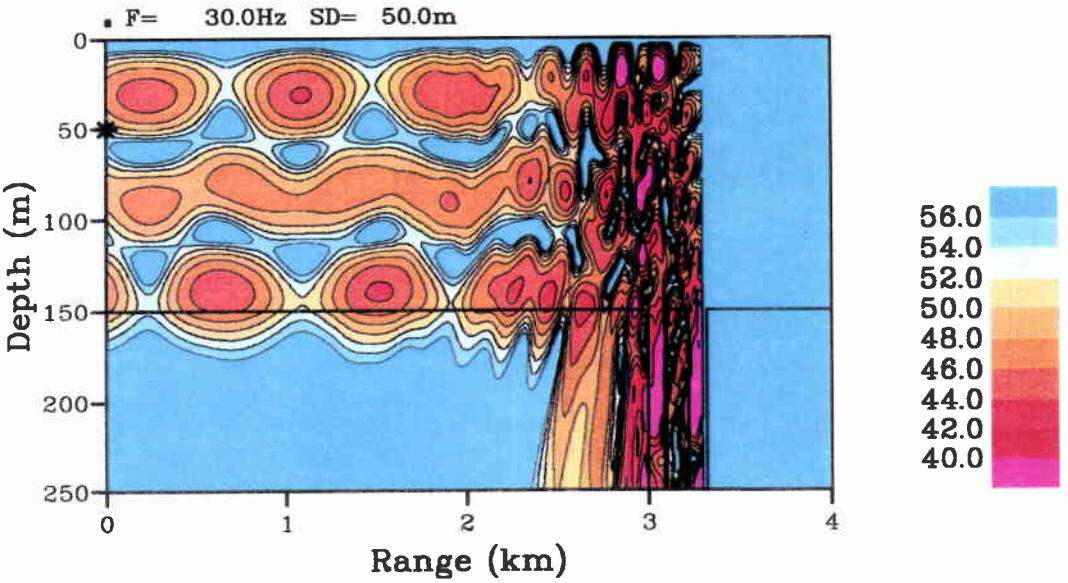

Figure 12 *Case 4a: Computed backscattered field from two bottom troughs placed 3 km downrange.*

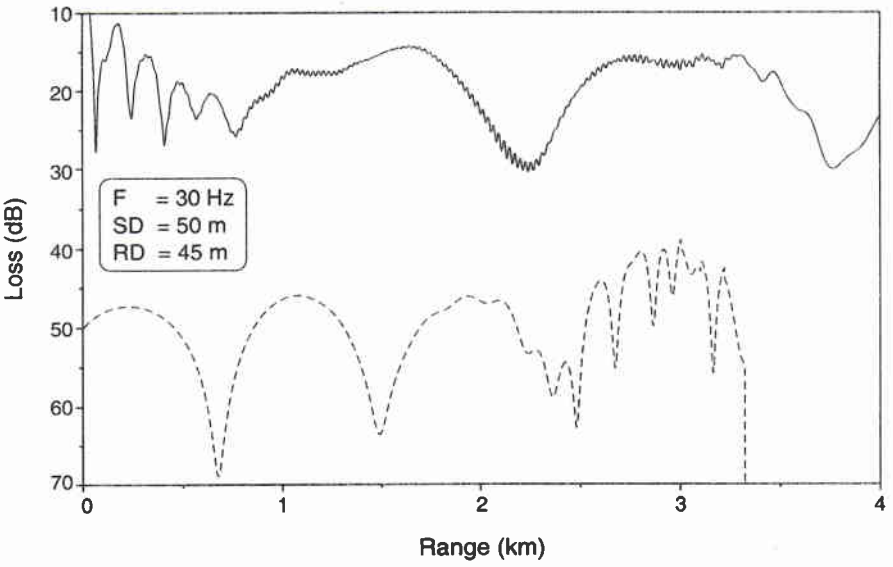

Figure 13 *Case 4a:* COUPLE *solutions for the total field (solid line) as well as the backscattered field component (dashed line).*

6
Case 5

As illustrated in Annex A, this problem is different in several aspects. First of all, the problem will be done for a point source in cylindrical geometry, and two boundary conditions at $r = 0$ are considered: (i) a radiating boundary without resonance in the horizontal, with receivers at 45 m (Case 5a) and 125 m (Case 5b), and (ii) a reflecting boundary with resonance (reverberation) in the horizontal, with receivers at 45 m (Case 5c) and 125 m (Case 5d). Also, the bottom properties differ from the earlier examples by having a higher density of 2.5 g/cm^3. The sound speed is still 1800 m/s and the attenuation 0.5 dB/λ.

The scatterer consists of an axisymmetric square-wave corrugated annulus extending from 2.0 to 2.5 km, see Fig. 14. The amplitude of the square-wave is ± 10 m and its wavelength is 50 m. Hence, there are 10 ridges and 10 troughs in the scattering patch.

Figure 15 shows the COUPLE solution for Case 5a (no resonance). Note the high backscatter level right above the scattering patch, which also gives rise to strong interference in the total field solution. The numerical convergence with the number of modes was very slow, and it was necessary to include a total of 100 modes to obtain numerically stable results. It is not clear whether it is the higher bottom density or multiple scattering effects that is responsible for the slow numerical convergence. As shown in Annex B, the solution for Case 5c with horizontal resonance only differs slightly from the result without resonance (Case 5a). Solutions for an alternative receiver depth of 125 m are also given in the annex.

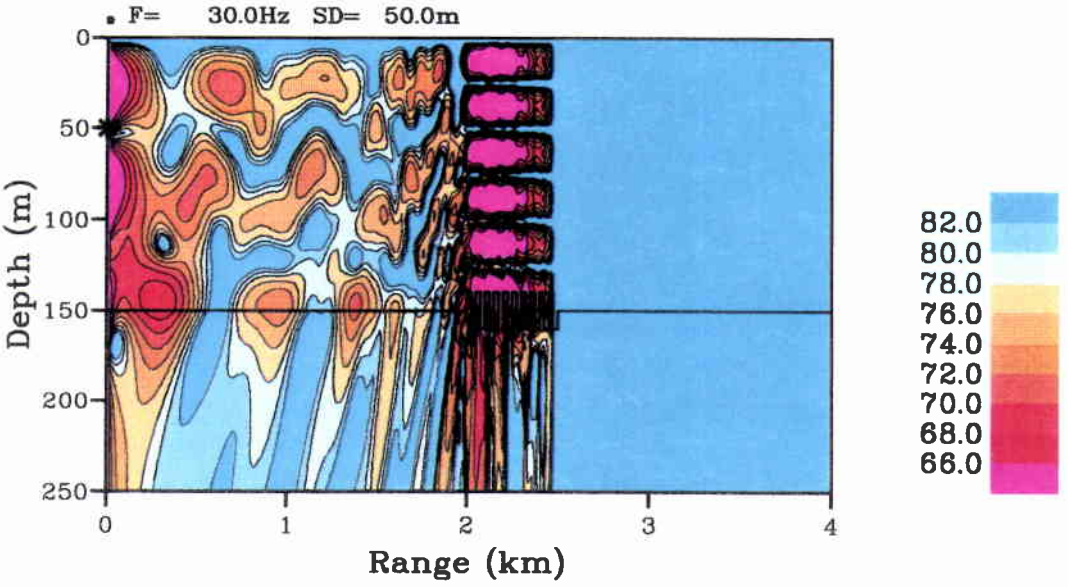

Figure 14 *Case 5a: Computed backscattered field from roughness patch placed 2 km downrange. Note that this problem is done in cylindrical geometry.*

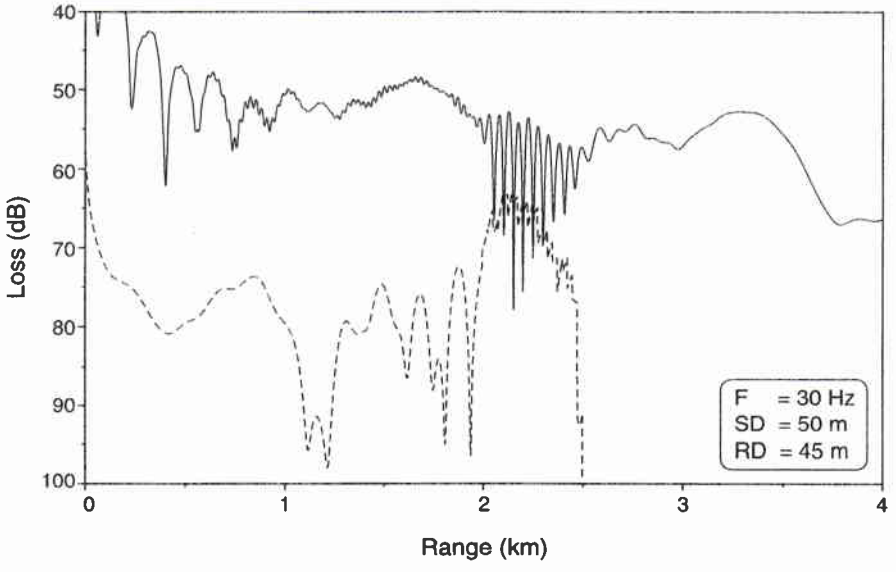

Figure 15 *Case 5a:* COUPLE *solutions for the total field (solid line) as well as the backscattered field component (dashed line).*

7

Broadband solutions

It might seem of limited interest to create benchmark solutions also in the time domain, since, having obtained accurate CW results for the various test problems, a broadband computation based on Fourier synthesis becomes entirely a matter of CPU time. However, there are numerical codes around that solve the scattering problem directly in the time domain, and these codes require broadband solutions for checking. Moreover, as discussed below, there are interesting computational issues associated with the Fourier synthesis technique in terms of obtaining accurate broadband results with minimum computational effort.

7.1. COMPUTATIONAL ISSUES

As specified in the Workshop announcement, time-series solutions were requested for Cases 2–5 at just two spatial positions: 5 m away from the source and 3.5 km downrange. The source pulse shown in Fig. 16 has a Gaussian spectrum of unit amplitude and width 10 Hz, centered at 30 Hz. The finite bandwidth used in the pulse synthesis was 10–50 Hz.

From the geometry of the problem we can easily estimate the required time window length. Thus, assuming the fastest arrival (mode 1) to move with the water sound speed of 1500 m/s, the signal backscattered from the obstacles 3 km downrange arrives back at the source range with a delay of $(2 \times 3000)/1500 = 4$ s. Taking into account also the signal dispersion in the waveguide it is clear that a time window of at least 5 s is required. To make sure that no signal wrap-around occurred in the Fourier synthesis, we used $T = 8$ s for the majority of the test problems.

The computational effort associated with generating a synthesized pulse is directly proportional to the number of frequency samples used. With a bandwidth of 40 Hz and a time window of 8 s ($\Delta f = 1/8$ Hz), we find the number of frequencies to be $\mathtt{NF} = 40 \times 8 = 320$. Of course, this number could be cut in half by taking a 30 Hz bandwidth (more noisy solutions) and limiting the time window to 5 s. In any event, a brute-force approach to solving the broadband problem with 320 frequencies and with the numerical parameters used for the CW results (Table 1) would lead to prohibitive CPU times in most cases.

As a first consideration in doing efficient broadband mode computations, we have to set up a scheme to ensure accurate results over the entire frequency band of 10–50 Hz. After some numerical testing, we opted for a scaling of both H_{B} and H_{A} with

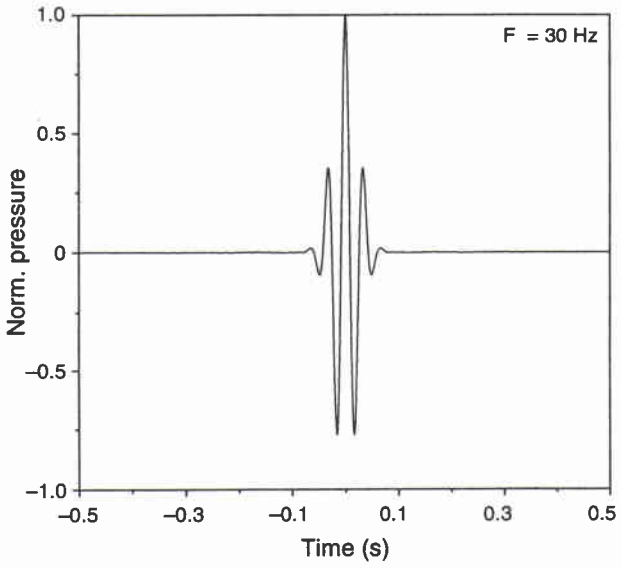

Figure 16 *Gaussian spectrum pulse for broadband calculations.*

the acoustic wavelength so that we have a deep false bottom and a thick attenuation layer at low frequencies, but much shallower depths at high frequencies. Since the number of modes in a problem (for a given source beamwidth) is proportional to both the false bottom depth H_B and the frequency, we can keep the number of modes fixed over the entire frequency band by scaling H_B with the acoustic wavelength. Hence, when indicating in Table 1 that broadband calculations are done with 25 modes, say, that means that 25 modes were used for all frequency computations between 10 and 50 Hz. On the other hand, the values shown for H_A and H_B refer to the center frequency, with a wavelength-dependent scaling applied across the band.

Numerical convergence tests for pulse solutions at 5 m and 3.5 km showed much less stringent requirements on false-bottom depth and range segmentation than experienced for the CW calculations. The reason is twofold: First of all, weak reflections off the false bottom may appear outside the time window of interest, and hence not disturb the solution. (Noise in CW calculations cannot be gated out.) Second, the pulse solution is requested at two ranges only and not right above the scatterer, where the accuracy constraints are most severe due to steep-angle propagation.

In summary, numerically stable time-series solutions were obtained with the parameters given in Table 1. Note that the false bottom depth of 500 m is only half of that used for the CW calculations, and so is the number of modes. The absorption layer extending from 300- to 500-m depth was taken to have a linearly increasing attenuation from 0.5 to 10.0 dB/λ. Finally, a range discretization `NSEG` = 21 was found to be sufficient for the rounded obstacles.

7.2. NUMERICAL RESULTS

Time-series solutions are presented in the form given in Fig. 17, i.e., as normalized pressure versus time. We here show the backscattered signal for Case 2a at a range of 5 m. The peak amplitude is 36.83 dB down compared to the amplitude of the source pulse. Note that the signal arrives with a delay of approximately 4 s, as estimated earlier. We also see that there is considerable dispersion leading to a signal length of around 0.7 s. The complete set of time-series solutions are available as full-page figures in Annex B.

Summary plots of pulse solutions are given in Figs. 18 and 19. The backscattered signal received at $R = 5$ m (Fig. 18) clearly reflects the nature of the scatterer, i.e., the signal is longer when two scatterers are involved (Cases 3 and 4 vs. Case 2), and the signal amplitude is low for the bottom troughs (Case 4) compared to the ridge cases (Cases 2 and 3). On the other hand, the rounding of the obstacle tops (Cases B vs. A) has little effect on the signal shape and amplitude.

The forward-scattered signal at $R = 3.5$ km is displayed in Fig. 19, with the reference signal pertaining to a waveguide without obstructions. Clearly, the nature of the scatterer (height, length, shape, etc.) is much less evident in these signals. Particularly signals 4A and 4C, which are almost identical to the reference, contain little information about the scatterer.

One of the purposes of Case 5 was to compute a truly reverberant signal in an axisymmetric environment with reflections at the source range. Such a solution is shown in Fig. 20 for Case 5c. In order to get a clean signal with minimum wrap-around, we increased here the time window to 32 s (1280 frequencies). Note the decaying amplitude of the reverberant signal with time. Six or seven reflections are evident, with a time separation of approximately 2.7 s corresponding to a round trip travel from the source to the scatterer (at 2 km) and back again.

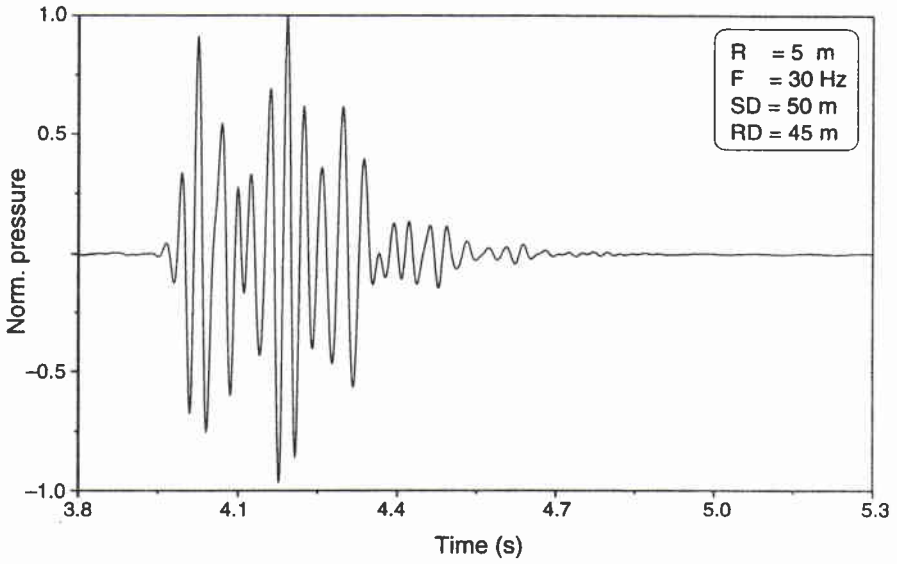

Figure 17 *Case 2a:* COUPLE *solution for the backscattered signal at a range of 5 m.*

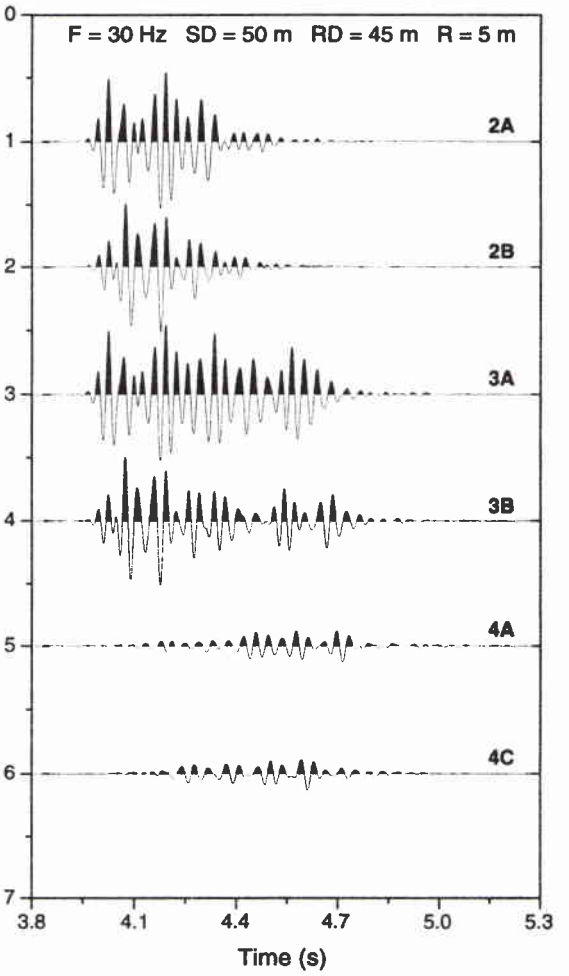

Figure 18 *Comparison of* COUPLE *solutions for the backscattered signal at range 5 m.*

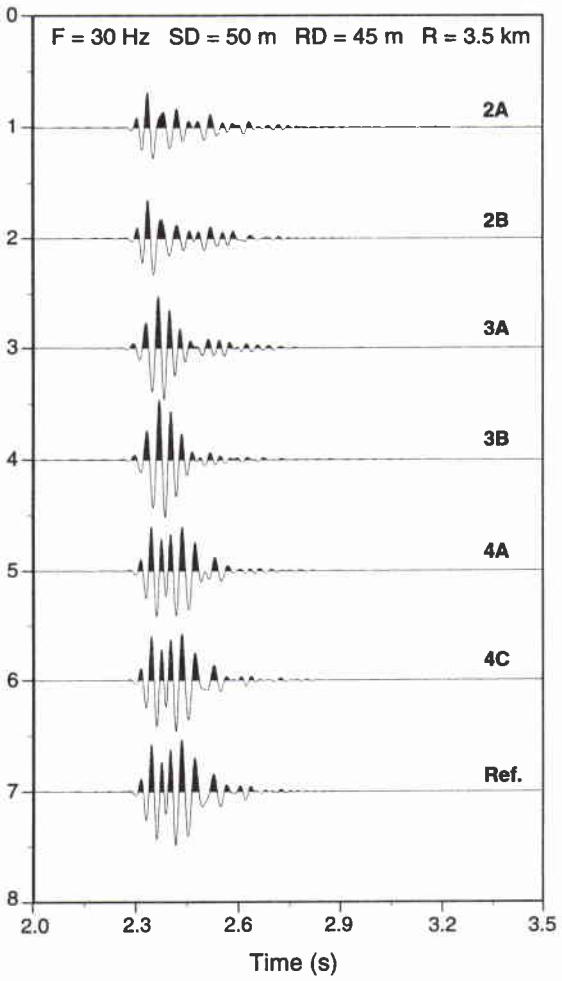

Figure 19 *Comparison of* COUPLE *solutions for the forward scattered signal at range 3.5 km. The reference signal is for a waveguide without obstructions.*

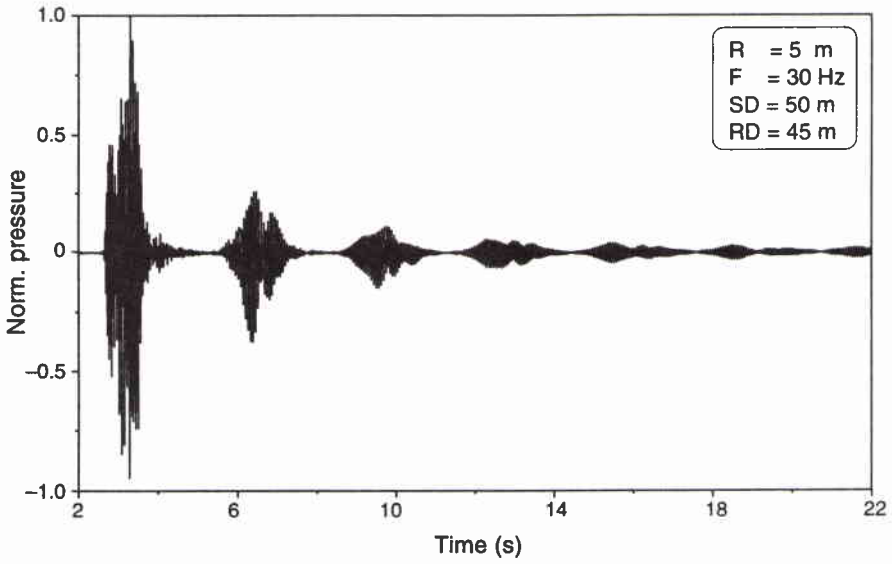

Figure 20 *Case 5c:* COUPLE *solution for the reverberant signal at range 5 m for a reflecting boundary condition at the source. The total time window is 32 s.*

8

Summary and conclusions

A series of test problems from the Reverberation and Scattering Workshop have been solved using different numerical codes. It was found that wide-angle PE codes are well-suited for studying forward scattering from a rough sea surface, with the computed field solution versus depth being in close agreement with the reference solution of Thorsos.

The set of problems dealing with backscattering from obstacles on the seafloor were all solved with the latest version of Evans' coupled-mode code (COUPLE). Numerically stable solutions (to within the line thickness of the graphical displays) were obtained for all test problems (CW and broadband), and results were found to be in close agreement with those obtained from a boundary-element code for selected problems. Considering further that the COUPLE code over the past decade has been used successfully to provide reference solutions to other benchmark problems in ocean acoustics, we feel confident that also the numerical results presented here for the feature-scattering problems are accurate solutions that can serve as references for future model validations.

References

[1] Jensen, F.B., Kuperman, W.A., Porter, M.B. and Schmidt, H. Computational Ocean Acoustics. New York, NY, American Institute of Physics, 1994. [ISBN 1-56396-209-8]

[2] Jensen, F.B. and Ferla, C.M. Numerical solutions of range-dependent benchmark problems in ocean acoustics. *Journal of the Acoustical Society of America*, **87**, 1990: 1499–1510.

[3] Chin-Bing, S.A., King, D.B., Davis, J.A. and Evans, R.B., *eds.* PE Workshop II: Proceedings of the Second Parabolic Equation Workshop. Naval Research Laboratory, Stennis Space Center, MS, 1993. [NRL/BE/7181-93-0001]

[4] Jensen, F.B. and Gerstoft, P. Benchmark solutions for backscattering in simple waveguide geometries. *In*: Proceedings of the second European Conference on Underwater Acoustics, volume I. Bjørnø, L., *ed.* Luxembourg, European Commission, 1994, pp. 119–124. [ISBN 92-826-7514-9]

[5] Chin-Bing, S.A., King, D.B., Davis, J.A. and Evans, R.B., *eds.* R&S Workshop: Proceedings of the Reverberation and Scattering Workshop. Naval Research Laboratory, Stennis Space Center, MS, 1995.

[6] Evans, R.B. A coupled mode solution for acoustic propagation in a waveguide with stepwise depth variations of a penetrable bottom. *Journal of the Acoustical Society of America*, **74**, 1983: 188–195.

[7] Evans, R.B. 'A reverberation calculation using stepwise coupled modes,' (in [5]).

[8] Lee, D., Botseas, G. and Papadakis, J.S. Finite-difference solution of the parabolic wave equation. *Journal of the Acoustical Society of America*, **70**, 1981: 795–800.

[9] Lee, D. and Botseas, G. IFD: An implicit finite-difference computer model for solving the parabolic equation, NUSC TR-6659. New London, CT, Naval Underwater Systems Center, 1982.

[10] Thomson, D.J. *In*:Chin-Bing, S.A., King, D.B., Davis, J.A. and Evans, R.B., *eds.* PE Workshop II: Proceedings of the Second Parabolic Equation Workshop. Naval Research Laboratory, Stennis Space Center, MS, 1993. [NRL/BE/7181-93-0001]

[11] Thorsos, E.I. *In*:Chin-Bing, S.A., King, D.B., Davis, J.A. and Evans, R.B., *eds.* PE Workshop II: Proceedings of the Second Parabolic Equation Workshop. Naval Research Laboratory, Stennis Space Center, MS, 1993. [NRL/BE/7181-93-0001]

[12] Gerstoft, P. and Schmidt, H. A boundary element approach to seismo-acoustic facet reverberation. *Journal of the Acoustical Society of America*, **89**, 1991: 1629–1642.

Annex A

Test problems

TEST CASE 1: Sea surface forward scattering

(Contributed By Eric Thorsos, (206) 543-1369,
email: eit@apl.washington.edu)

This test case is a rough sea surface scattering problem assuming an isovelocity medium and a cw wave field. The problem is restricted to a 1-D rough surface, and therefore the field is only a function of range and depth. The rough surface profile is specified at range intervals of wavelength/10. The field incident on the rough surface is given as a function of depth at the left endpoint of the surface (range 0) in the form of a tapered plane wave. The incident field is also given on the rough surface profile itself so that either form of the incident field can be used. For this problem the incident field is not negligible at the right endpoint of the surface and therefore the incident field will also be given as a function of depth at the right endpoint of the surface; this will be needed if the problem is solved using the incident field specified on the rough surface profile. The solution for the complex total field (incident plus scattered) will be given as a function of depth at the right endpoint of the surface. The solution will be obtained using an integral equation method.

Problem parameters:

The frequency is 400 Hz (a wavelength of 3.75 m).

The rough surface is constructed to be consistent with a 1-D Pierson-Moskowitz spectrum for a wind speed of 15 m/s. The total surface length is 750 m. The surface height, first derivative, and second derivative will be provided at 2000 equally spaced points on the range axis (a spacing of 0.375 m).

The mean grazing angle for the incident field is 10 deg. The field is spatially tapered and is centered on the surface. The field is defined by its values as a function of depth at range 0, where it is specified by a simple analytic form, i.e., a Gaussian tapered plane wave. The exact incident field on the rough surface profile and (as a function of depth) at the right endpoint of the surface will be obtained using a Green's function method and provided for use, if desired. The precise analytic form at range 0 will be given when the rough surface file and the incident field files are provided.

Four files are provided [surface.tc1, inc_surface.tc1, inc_rep.tc1, solution.tc1]. If the solution is obtained by a marching method, as in the PE method, then only the surface and solution files are needed. This will be referred to as Method 1. If the solution method requires knowing the incident field on the rough surface, then all four files are needed; this will be referred to as Method 2.

"surface.tc1" file

Column 1: range (m)
Column 2: surface height profile (m)
Column 3: first derivative of surface profile
Column 4: 2nd derivative (1/m)

A positive value of surface height is above the mean surface. The convention has been used that the z axis is directed upward; thus depth = -z.

The surface is partitioned into 2000 intervals of length 0.375 m, and the surface values are given at the midpoints of each interval. The left endpoint of the entire surface is at range 0 m and the right endpoint is at range 750 m.

The frequency is 400 Hz (a wavelength of 3.75 m), so the surface intervals are of length wavelength/10.

"solution.tc1" file

The solution for the total field (incident plus surface scattered) is given as a function of z at the right endpoint of the surface (range 750 m).

Column 1: z value of field point
Column 2: real part of field
Column 3: imaginary part of field
Column 4: magnitude of field
Column 5: phase of field (in deg)

A time convention of exp[-i*omega*t] is assumed. The total field does not vanish at z = 0 because near the right endpoint the surface height is near 1.2 m. The boundary condition requires that the total field vanish on the rough surface.

Method 1

For a solution using Method 1, all that remains to be specified is the form of the field incident as a function of z at the left endpoint of the surface. This form is given by

p(z) = g(z)* exp[i*k*sin(theta)*z] , where k = 2(pi)/3.75m, theta = 10 deg, and

g(z) = exp{-[(z - zs)**2]/[g**2]} , where zs = -66.12 m and g = 27.55 m.

Method 2

For Method 2, the incident field is needed on the rough surface profile. This has been found using a Green's function method. File inc_surface.tc1 provides the incident field on the rough surface as a function of range.

"inc_surface.tc1" file

Column 1: range (m)
Column 2: real part of incident field on surface
Column 3: imaginary part of incident field on surface

When using Method 2 one typically computes the scattered field, not the total field. However, the total field is given directly by marching methods and also shows the effect of the boundary condition near the surface. Thus, the total field has been chosen as the

point of comparison. It turns out that the incident field is not completely negligible near the surface at the right endpoint, and therefore it must be added to the scattered field to obtain the total field.

File inc_rep.tc1 gives the incident field as a function of z at the right endpoint of the surface (range 750 m).

"inc_rep.tc1" file

Column 1: Index
Column 2: z value of field point
Column 3: real part of incident field at right endpoint of surface
Column 4: imaginary part of incident field at right endpoint
Column 5: magnitude of incident field
Column 6: phase (in deg) of incident field

TEST CASE 2: Backscatter from a penetrable step-like discontinuity.

This test case is intended to test the accuracy of discretized codes when the scattering surface is continuously varying in height and range. A rectangular or rounded object (See following figure) of height 100 m and width 120 m is place at a range of 3 km from the source. The water depth at the source is 150 m. The water sound speed is a constant 1500 m/sec. The bottom is a half space with a sound speed of 1800 m/sec, a density of 1.5 g/cc and an attenuation of 0.5 dB/wavelength.

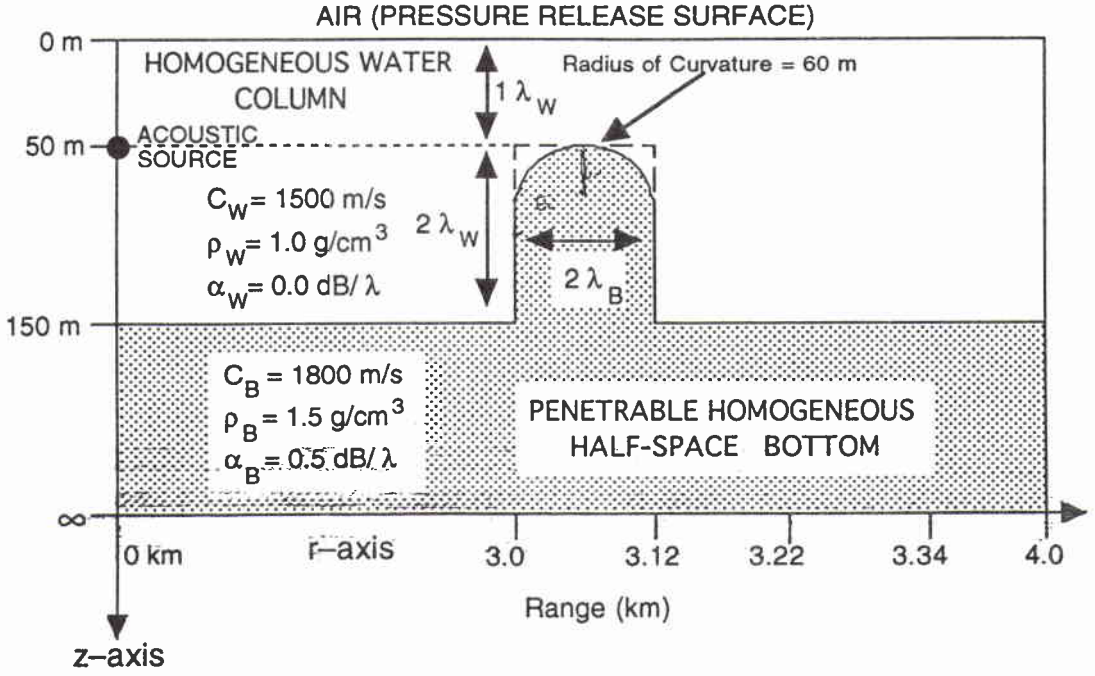

The dimensions of the discontinuity (height and width) are defined by wavelength multiples of the center frequency of 30 Hz (i.e., 50 m and 60 m respectively) as shown in the figure.

Participants are to solve Test Case 2 for two scenarios:

Case 2a: the flat protrusion, i.e., with the flat endcap

Case 2b: the rounded protrusion, i.e., with the half-cylinder endcap (radiius of curvature = 60 m).

Source/Receiver Parameters: Center Frequency = 30 Hz
Source Depth = 50 m
Receiver Depth = 45 m

For the predefined gaussian pulse, generate the time series for the total, outgoing, and backscattered pressures at ranges 5.0 meters and 3.5 km.

TEST CASE 3: Backscatter from adjacent penetrable step-like discontinuities.

This test case is intended to test the ability of backscatter codes to accurately handle multiple scattering when the scattering surfaces are continually varying in height and range. The following schematic figure illustrates Test Case 3.

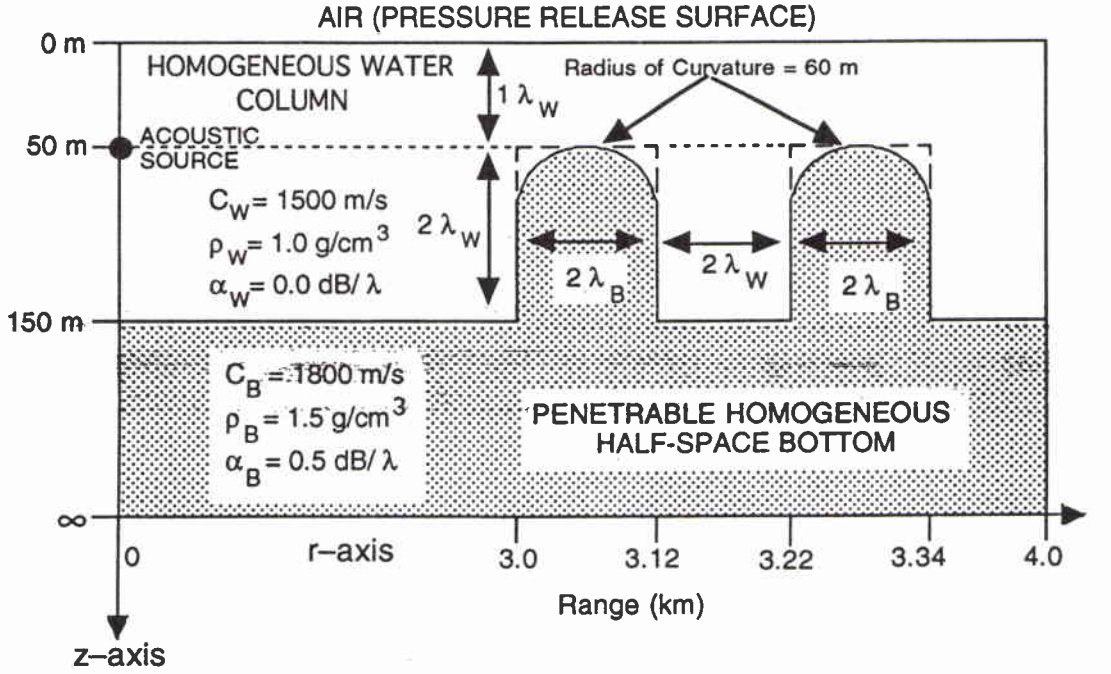

Test Case 3 is very similar to Test Case 2. In this case an additional scattering object has been added to the environments of Test Case 2. The leading edge of a second rectangular scattering object is placed 100 m from the trailing edge of the first rectangular object. Each rectangular or rounded object has a height 100 m and a width 120 m. The first object is placed at a range of 3 km The water depth at the source is 150 m. The water sound speed is a constant 1500 m/sec. The bottom is a half space with a sound speed of 1800 m/sec, a density of 1.5 gm/cc and an attenuation of 0.5 dB/wavelength.

Participants are to solve Test Case 3 for two scenarios:

Case 3a: two flat protrusions, i.e., with the flat endcaps

Case 3b: two rounded protrusions, i.e., with the half-cylinder endcaps (radii of curvature = 60 m).

Participants are to solve the above scenario for both cases, i.e., for the two flat protrusions and for the two rounded protrusions.

Source/Receiver Parameters: Center Frequency = 30 Hz
Source Depth = 50 m
Receiver Depth = 45 m

Obtain the following results: total, outgoing, and backscattered pressure in dB vs. range.

For the predefined gaussian pulse, generate the time series for the total, outgoing, and backscattered pressures at ranges of 5.0 meters and 3.5 km.

TEST CASE 4: Backscatter from adjacent penetrable trough discontinuities.

This test case is intended to test the ability of backscatter codes to accurately handle multiple scattering when the scattering surfaces are "holes" in the seafloor. Typically, reverberation is assumed to come from bathymetry that extend into the water column. This problem illustrates that reverberation can occur from any discontinuity in the seafloor.

The water column and bottom have the same properties as Test Cases 2 and 3. Two widths of the holes should be considered. For the cases 4a and 4b the width X should be set to 100 m and the receiver depths set at 45 m and 125 m, respectively. For the cases 4c and 4d the width of the holes X should be set to 60 m for receiver depths of 45 m and 125 m, respectively.

Source/Receiver Parameters: Center Frequency = 30 Hz
Source Depth = 50 m
Receiver Depths = 45 m and 125 m

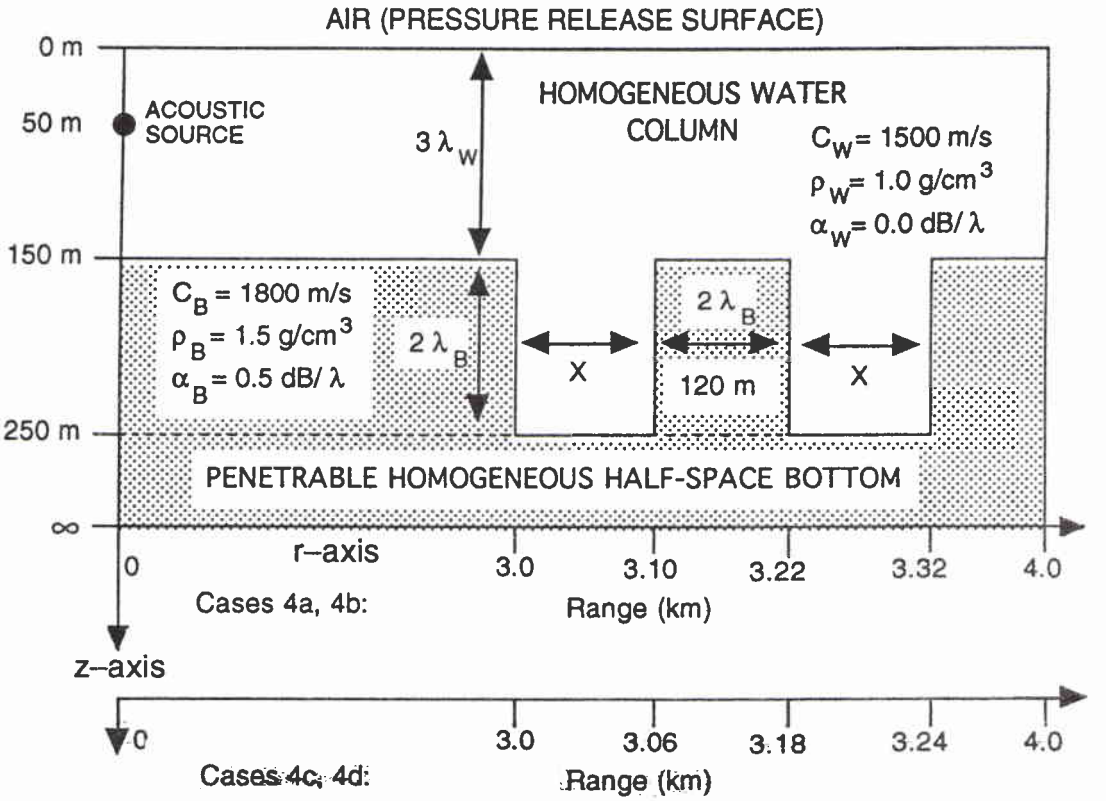

Obtain the following results: total, outgoing, and backscattered pressure in dB vs. range.

For the predefined gaussian pulse, generate the time series for the total, outgoing, and backscattered pressures at ranges of 5.0 meters and 3.5 km.

Because of the low level of the backscattered energy it is requested that the limits on the dB axis be increased by 20 dB.

TEST CASE 5: Reverberation from a penetrable, cylindrically axisymmetric, square-wave corrugated seafloor patch.

This test case is designed to test the ability of reverberation codes to accurately handle reverberation from a rough, penetrable seafloor patch. A cylindrical axisymmetric square-wave corrugated annulus is placed as shown in the figure. Reverberation from the annulus will focus at the axisymmetric axis.

Source/Receiver Parameters: Center Frequency 30 Hz
Source Depth = 50 m (on z–axis)
Receiver Depths = 45 m and 125 m (on z–axis)

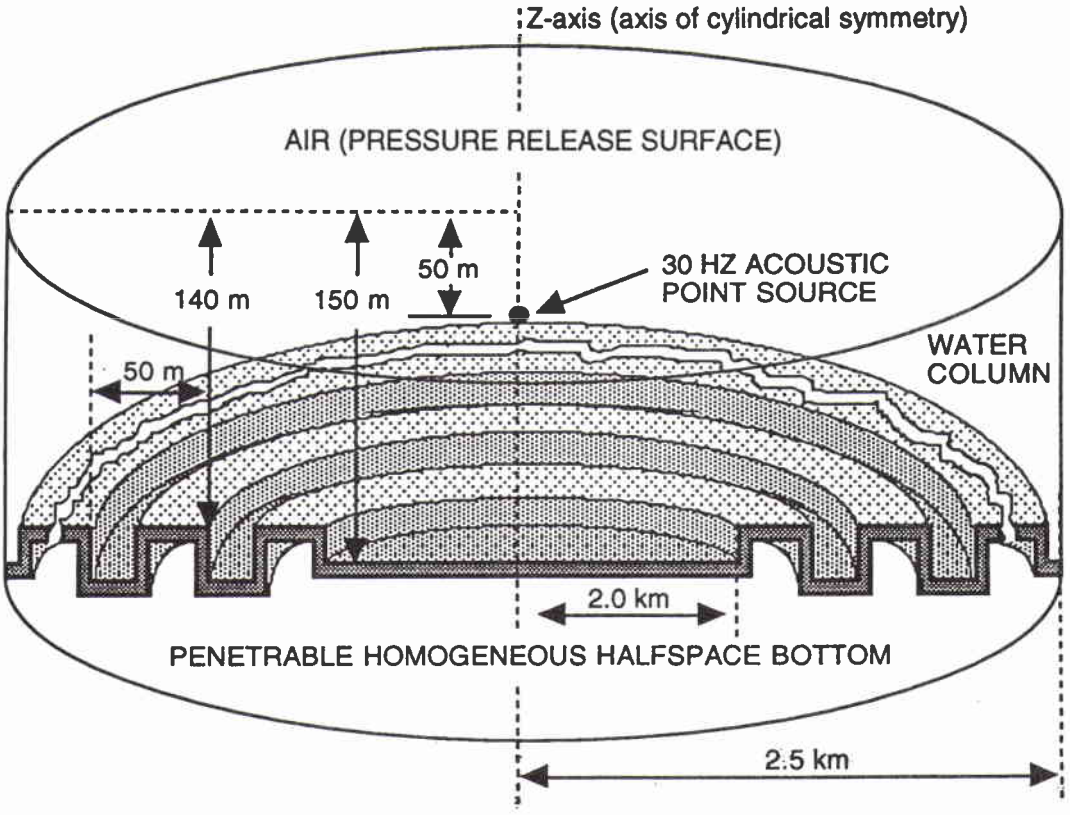

Parameters for the axisymmetric, square-wave corrugated annulus:

Length of square-wave over 1 period = 50 m
Amplitude of square-wave = ± 10 m
Number of periodic lengths in square-wave (N) = 10
Radial extent of corrugations = 500 m (2.0 to 2.5 km)

The environmental parameters are the same as in the previous test cases, i.e.,

In the water column: C_w = 1500 m/s
Density = 1.0 g/cm^3
Attenuation = 0.0

In the penetrable homogeneous half-space bottom:
C_b = 1800 m/s
Density = 2.5 g/cm^3
Attenuation = 0.5 dB/λ

Obtain the following results: total, outgoing, and backscattered pressure in dB vs. range.

For the predefined gaussian pulse, generate the time series for the total, outgoing, and backscattered pressure at ranges of 0.0 meters and 3.5 km.

Annex B
Solutions

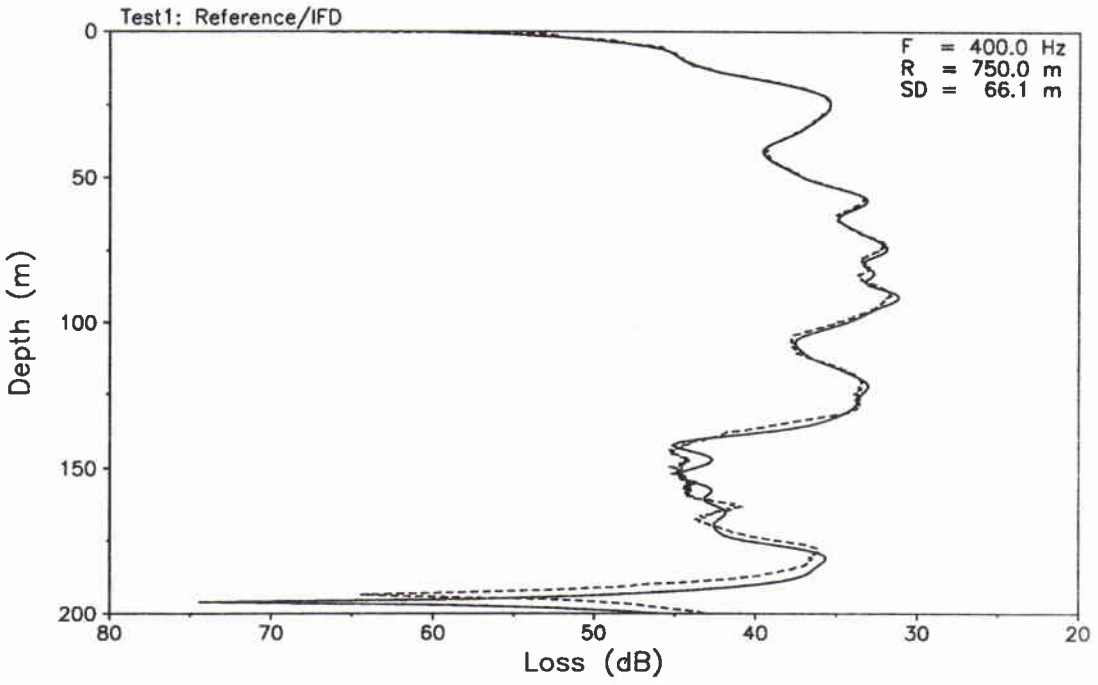

Figure B1 Case 1: Comparison of reference solution (solid line) with IFD result (dashed line).

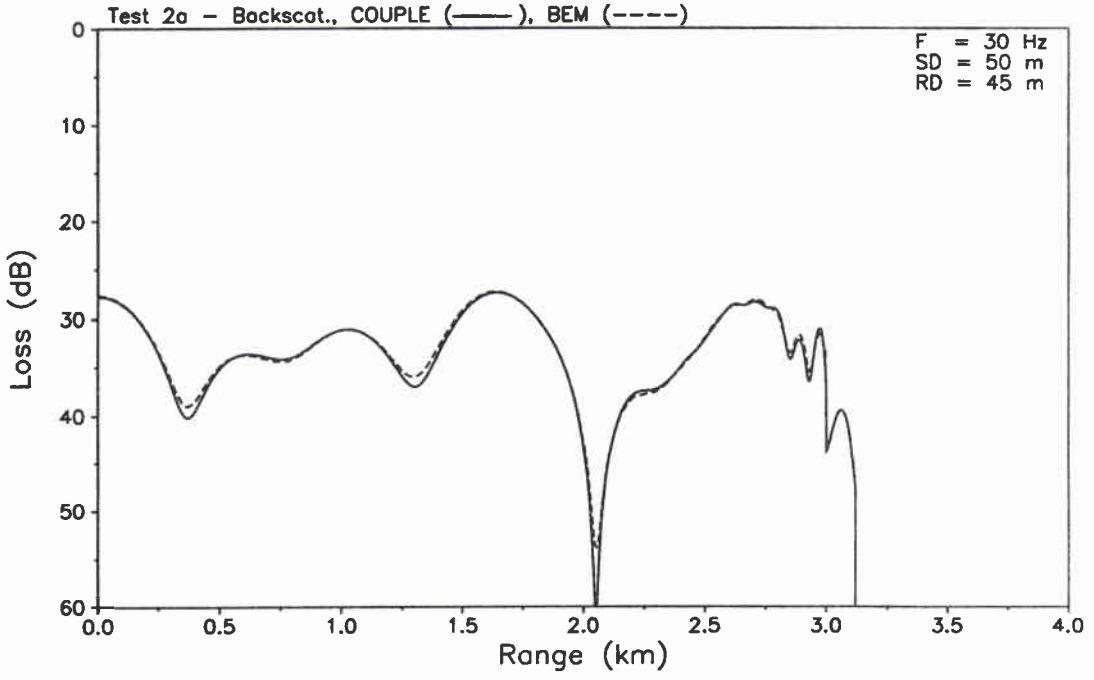

Figure B2 Case 2a: Comparison of COUPLE solution (solid line) with BEM result (dashed line).

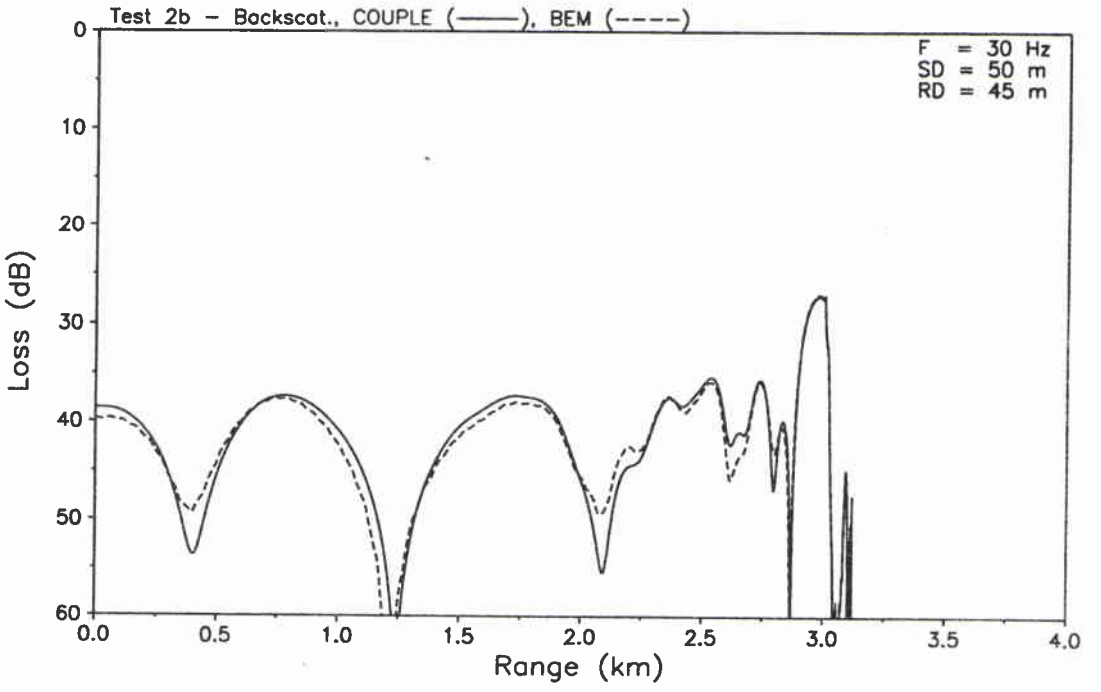

Figure B3 Case 2b: Comparison of COUPLE solution (solid line) with BEM result (dashed line).

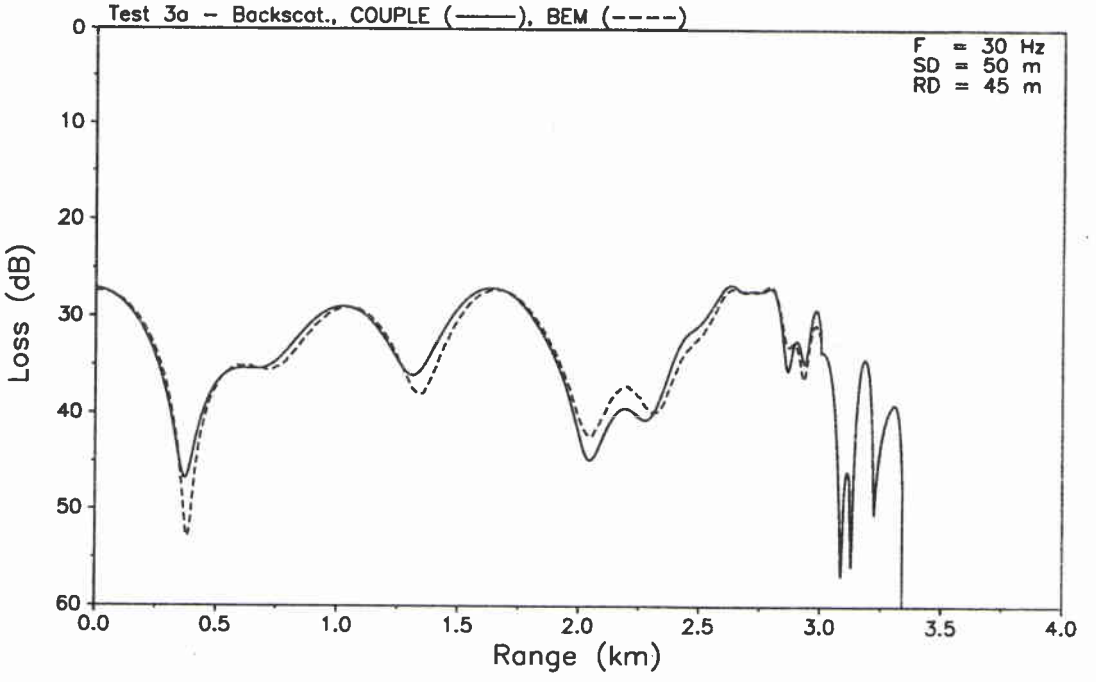

Figure B4 Case 3a: Comparison of COUPLE solution (solid line) with BEM result (dashed line).

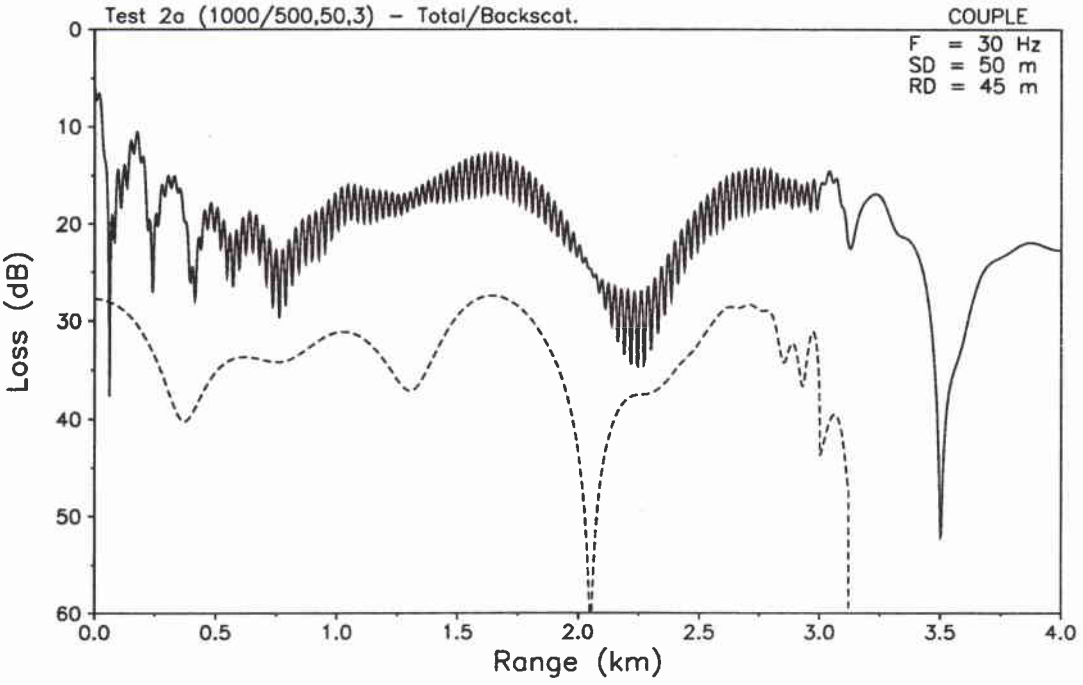

Figure B5 Case 2a: COUPLE solutions for the total field (solid line) as well as the backscattered field component (dashed line).

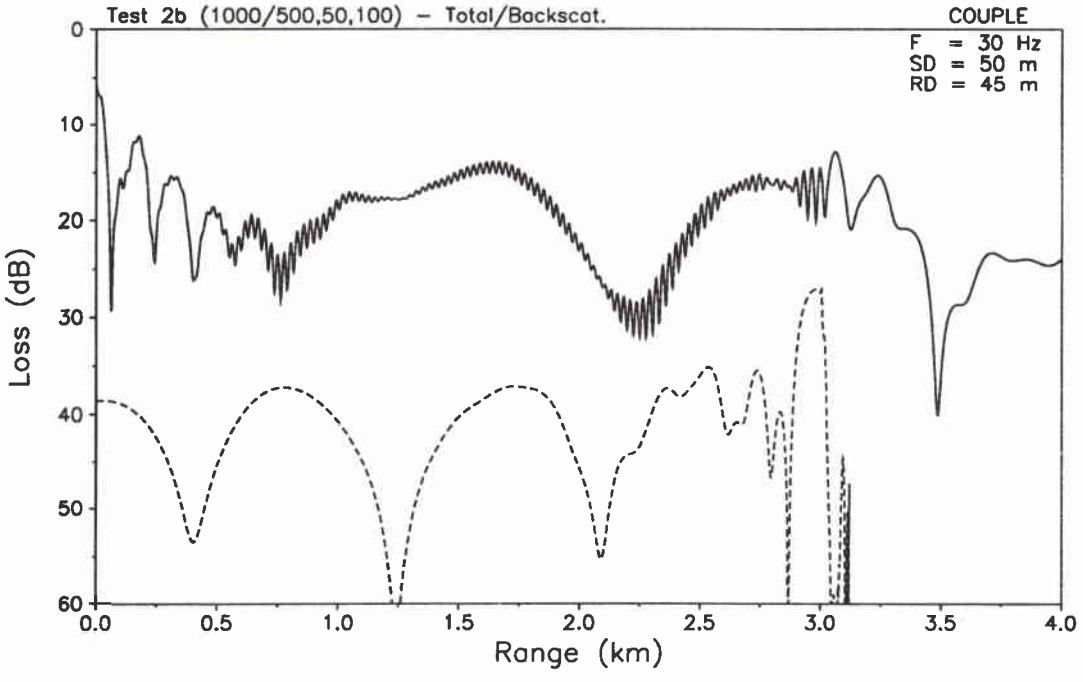

Figure B6 Case 2b: COUPLE solutions for the total field (solid line) as well as the backscattered field component (dashed line).

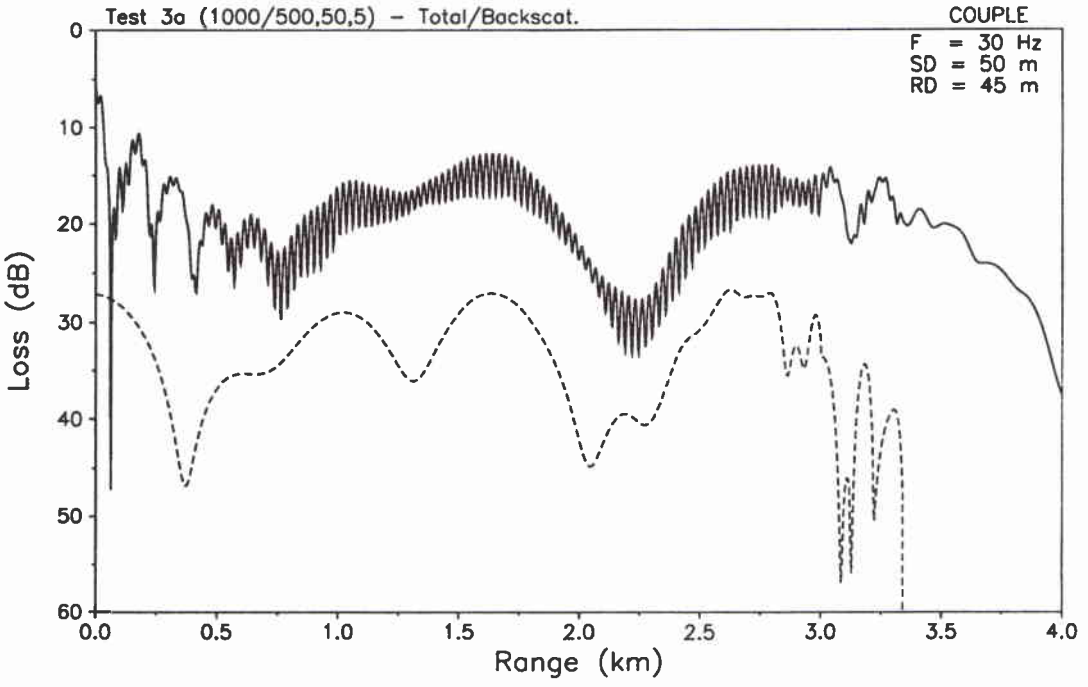

Figure B7 Case 3a: COUPLE solutions for the total field (solid line) as well as the backscattered field component (dashed line).

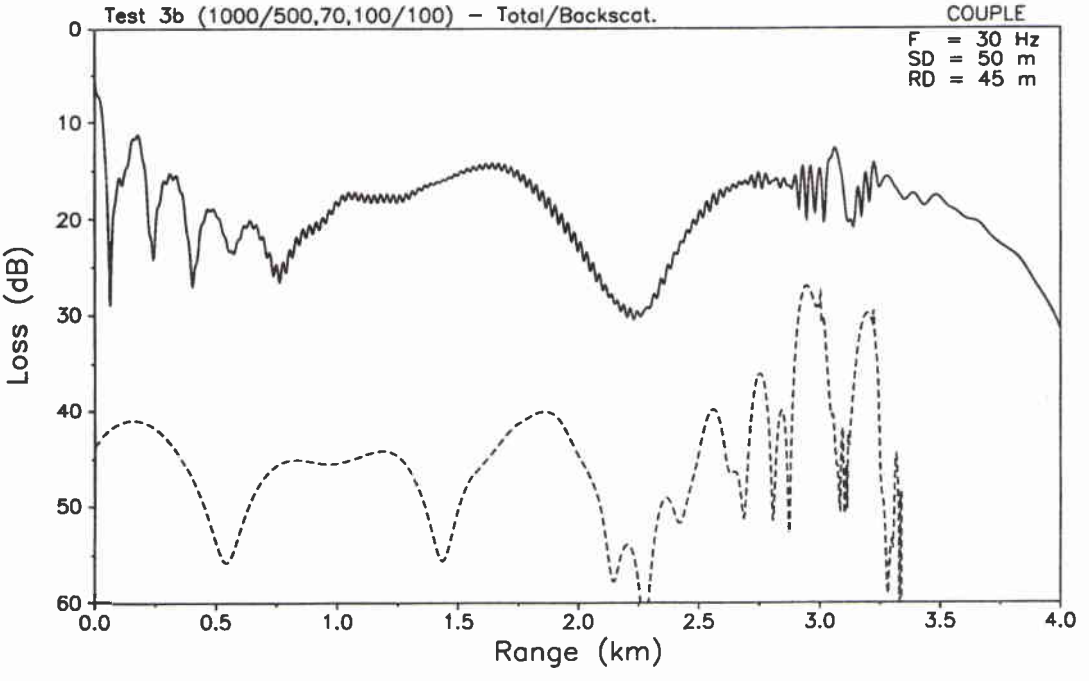

Figure B8 Case 3b: COUPLE solutions for the total field (solid line) as well as the backscattered field component (dashed line).

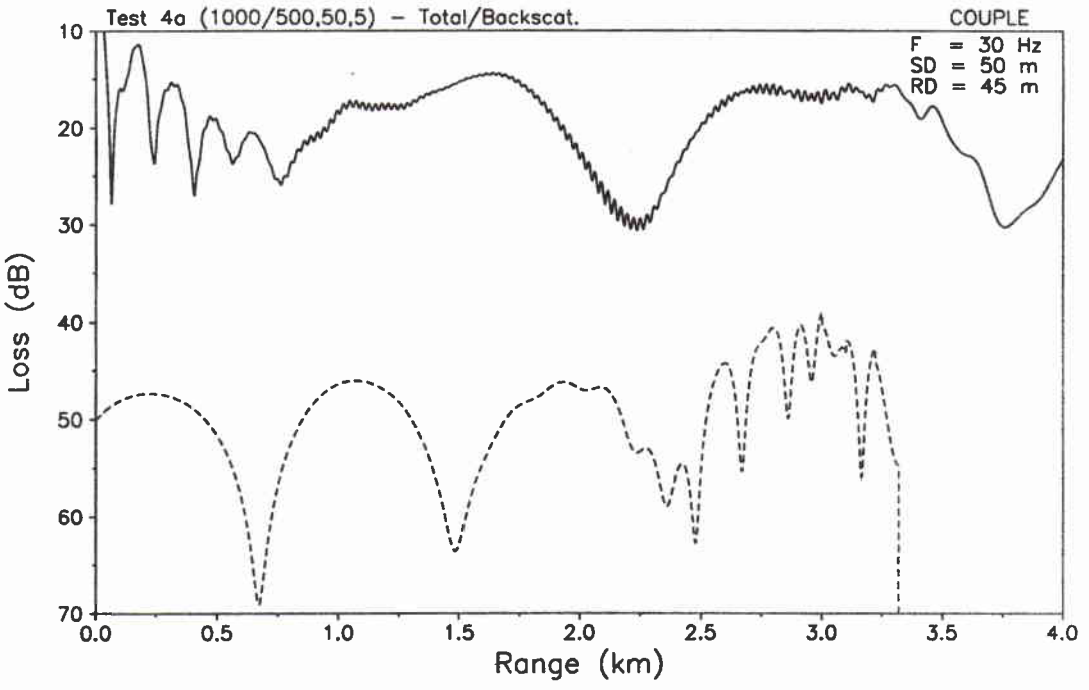

Figure B9 Case 4a: COUPLE solutions for the total field (solid line) as well as the backscattered field component (dashed line).

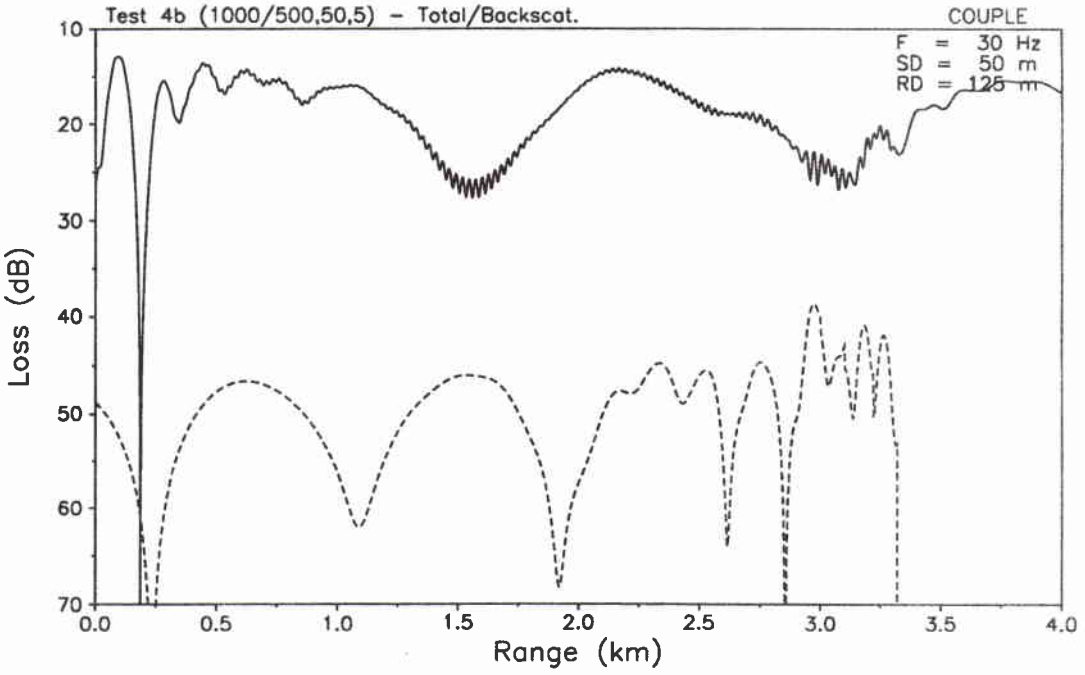

Figure B10 Case 4b: COUPLE solutions for the total field (solid line) as well as the backscattered field component (dashed line).

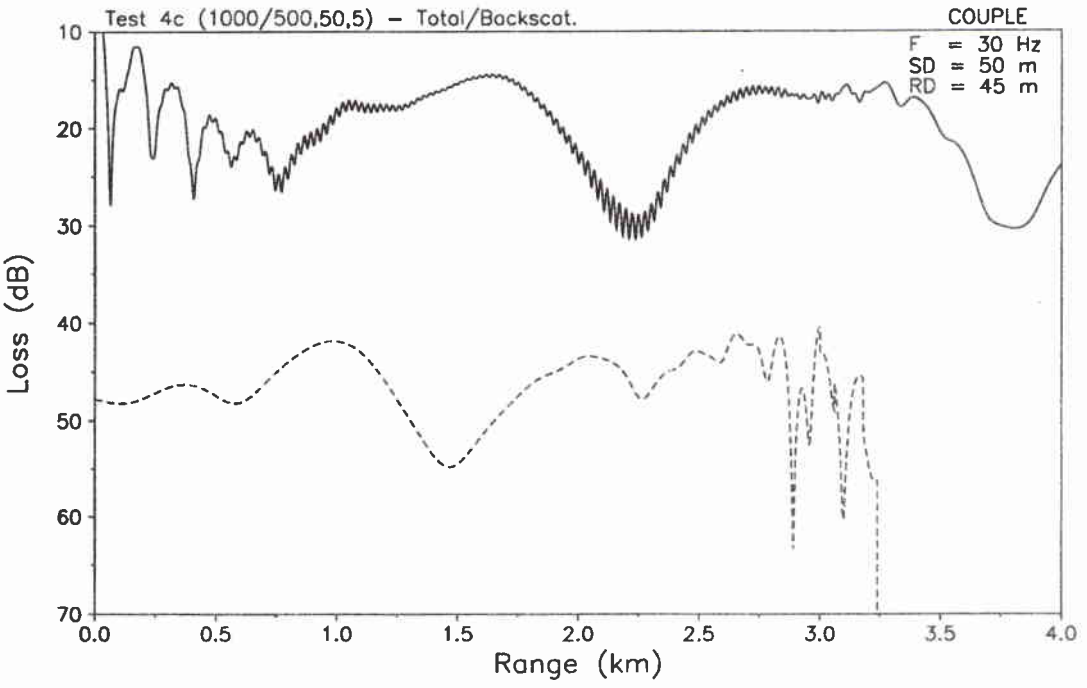

Figure B11 Case 4c: COUPLE solutions for the total field (solid line) as well as the backscattered field component (dashed line).

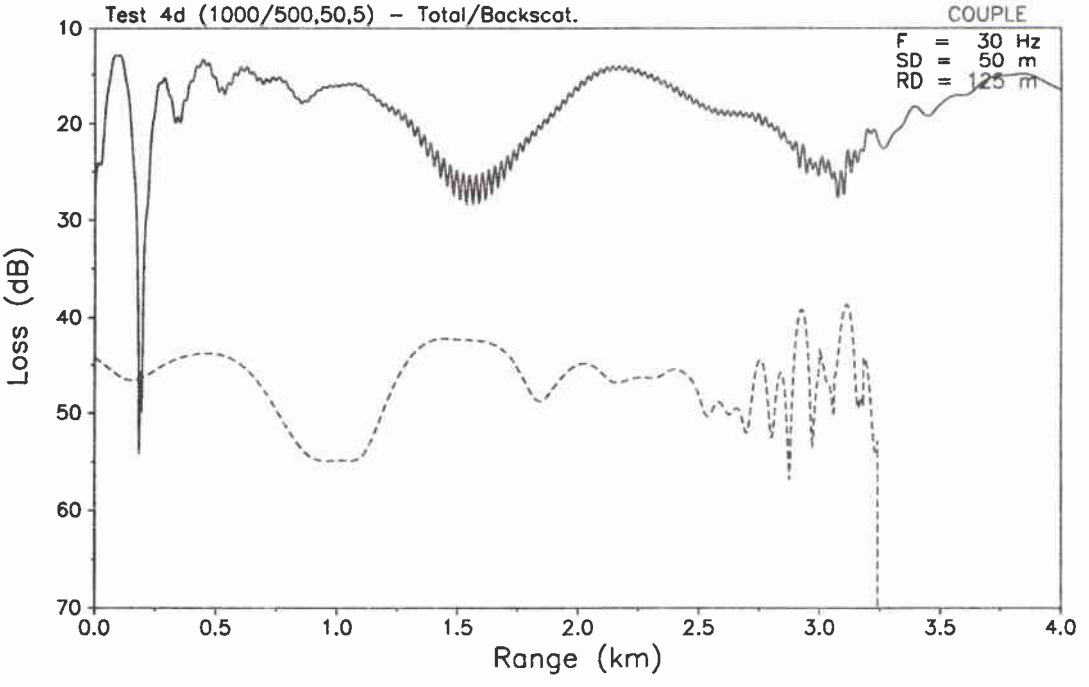

Figure B12 Case 4d: COUPLE solutions for the total field (solid line) as well as the backscattered field component (dashed line).

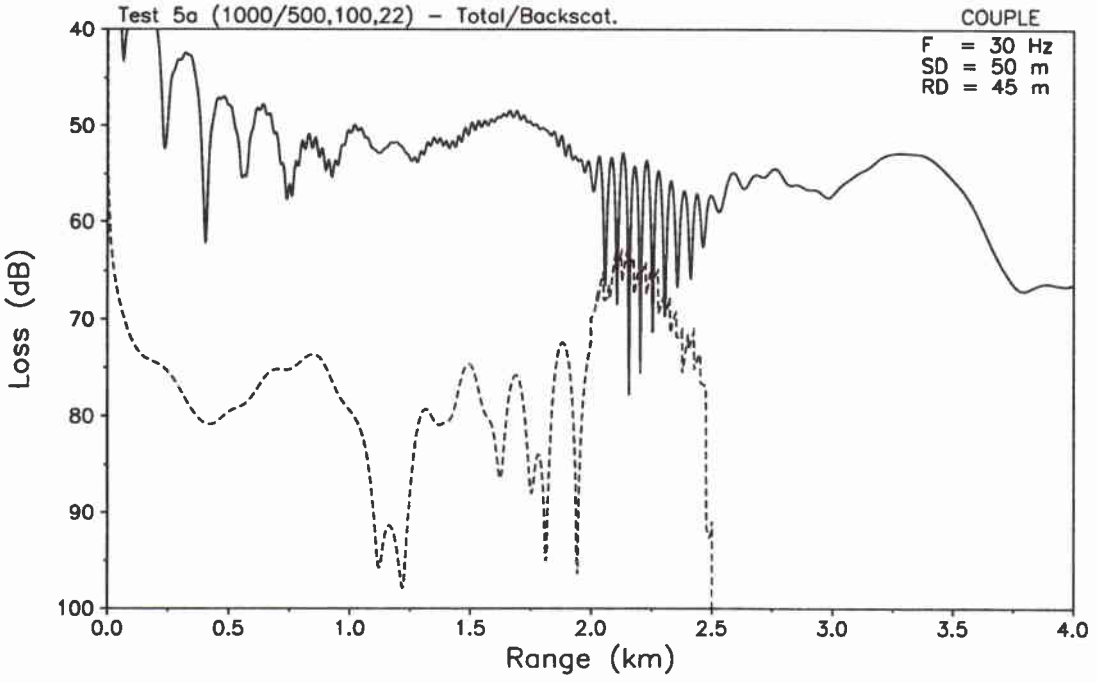

Figure B13 Case 5a: COUPLE solutions for the total field (solid line) as well as the backscattered field component (dashed line).

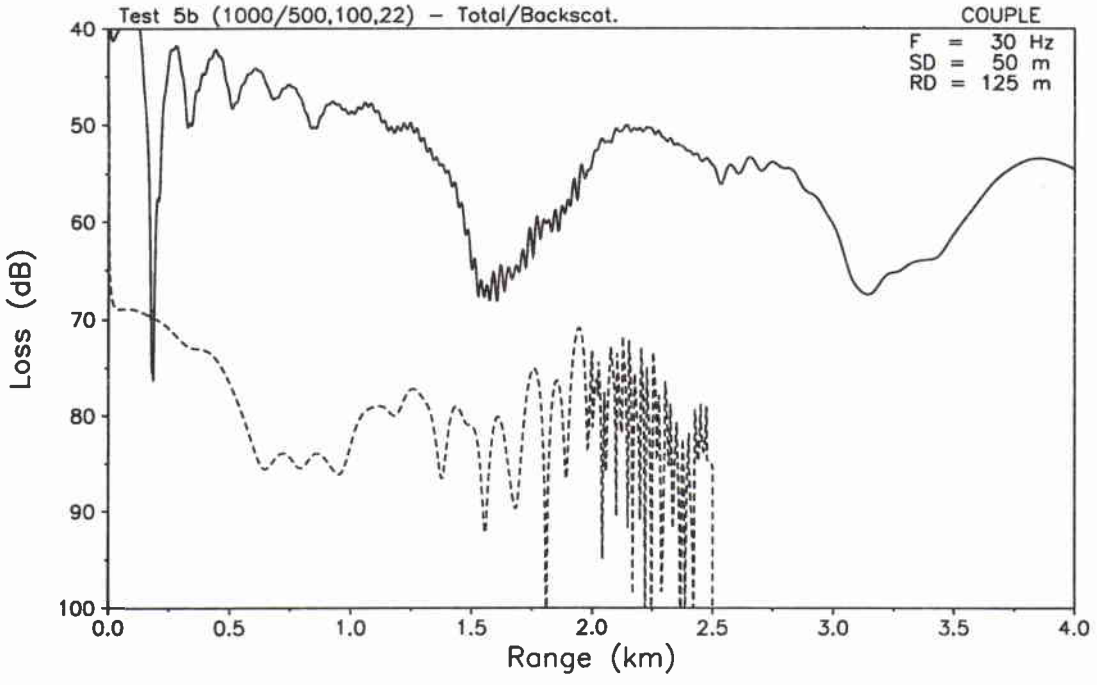

Figure B14 Case 5b: COUPLE solutions for the total field (solid line) as well as the backscattered field component (dashed line).

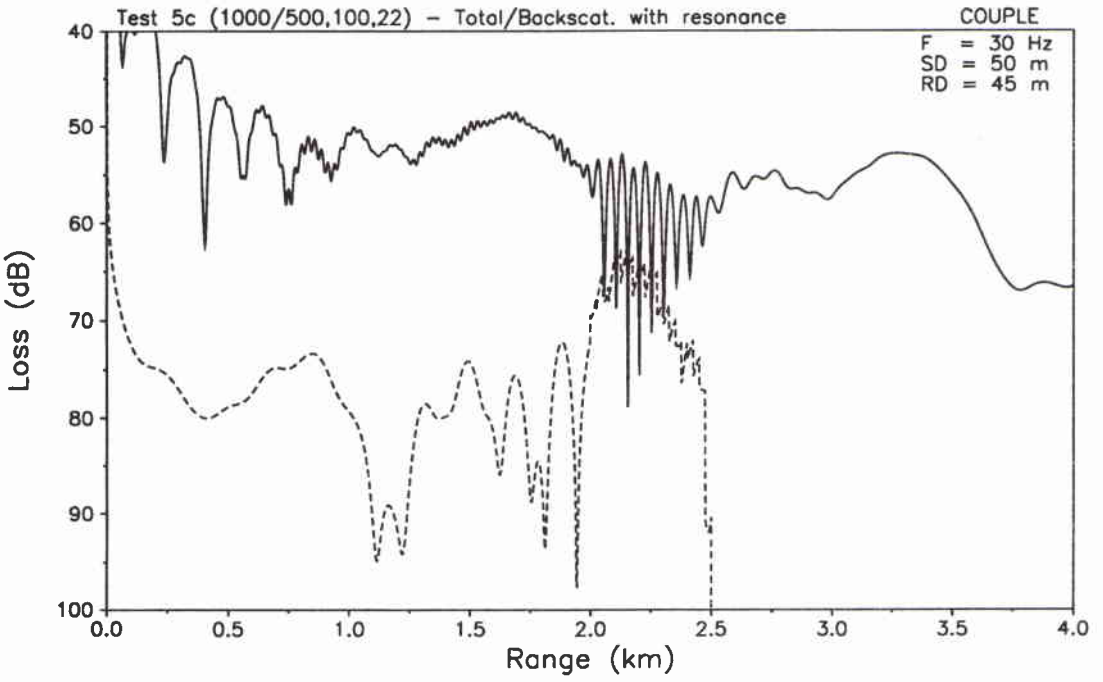

Figure B15 Case 5c: COUPLE solutions for the total field (solid line) as well as the backscattered field component (dashed line).

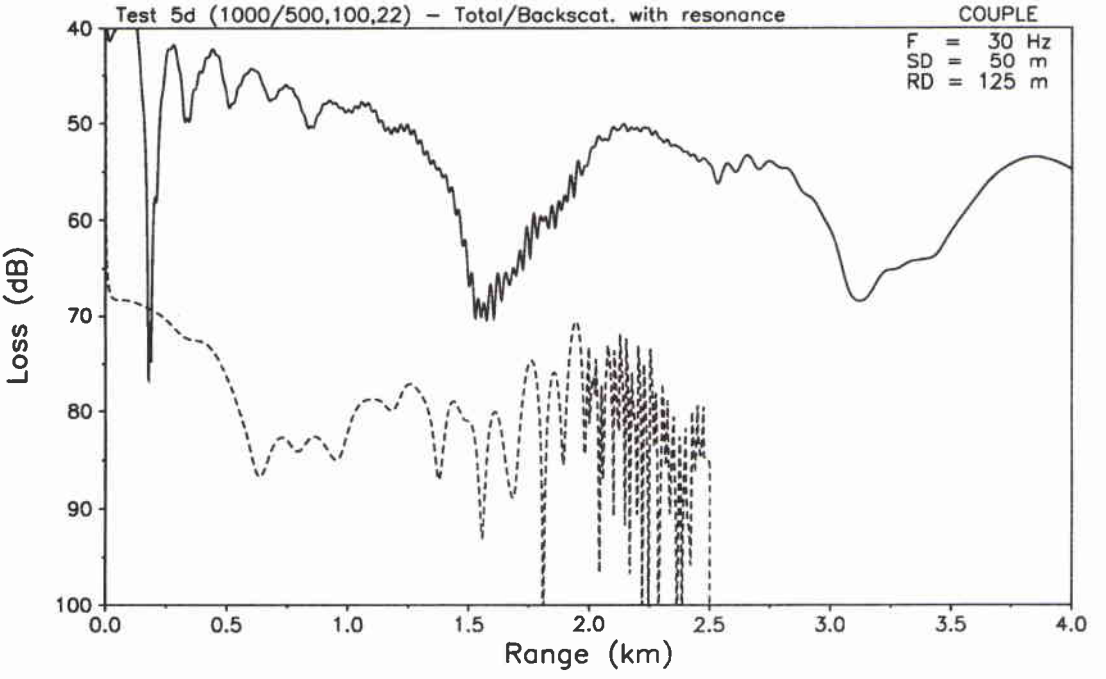

Figure B16 Case 5d: COUPLE solutions for the total field (solid line) as well as the backscattered field component (dashed line).

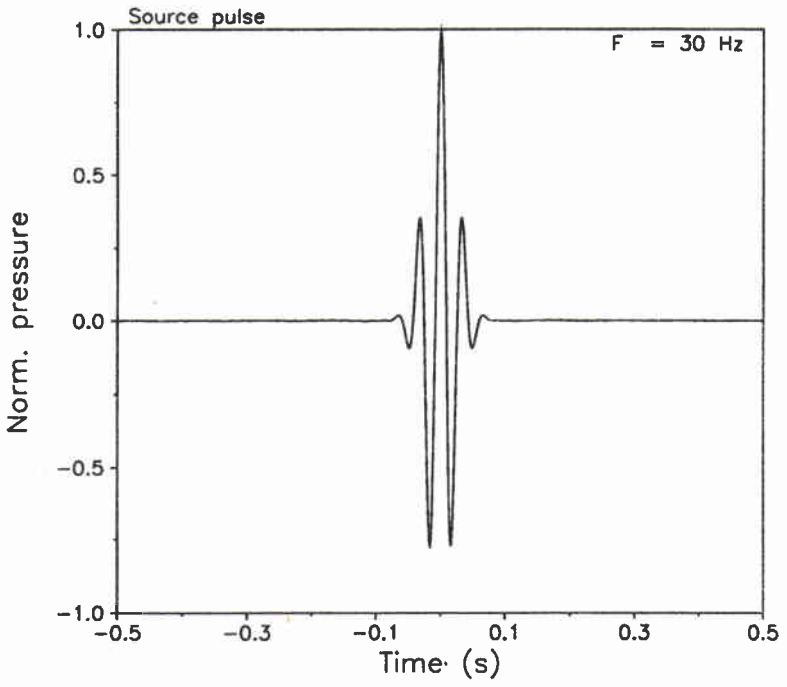

Figure B17 Gaussian-spectrum pulse for broadband calculations.

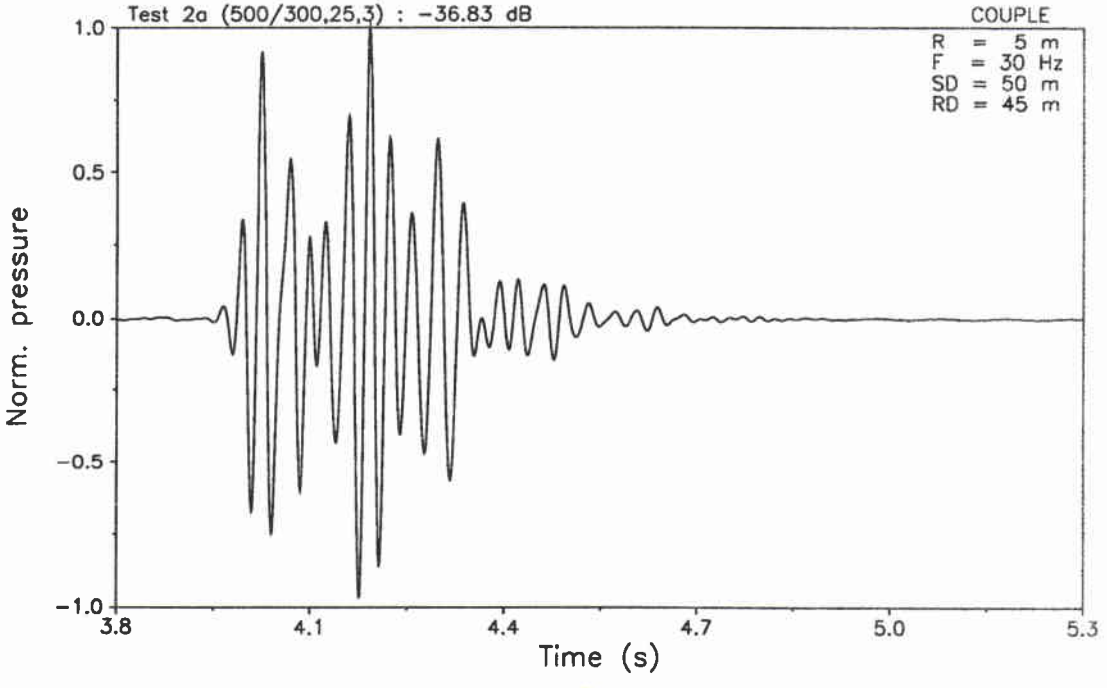

Figure B18 Case 2a: COUPLE solution for the backscattered signal at range 5 m.

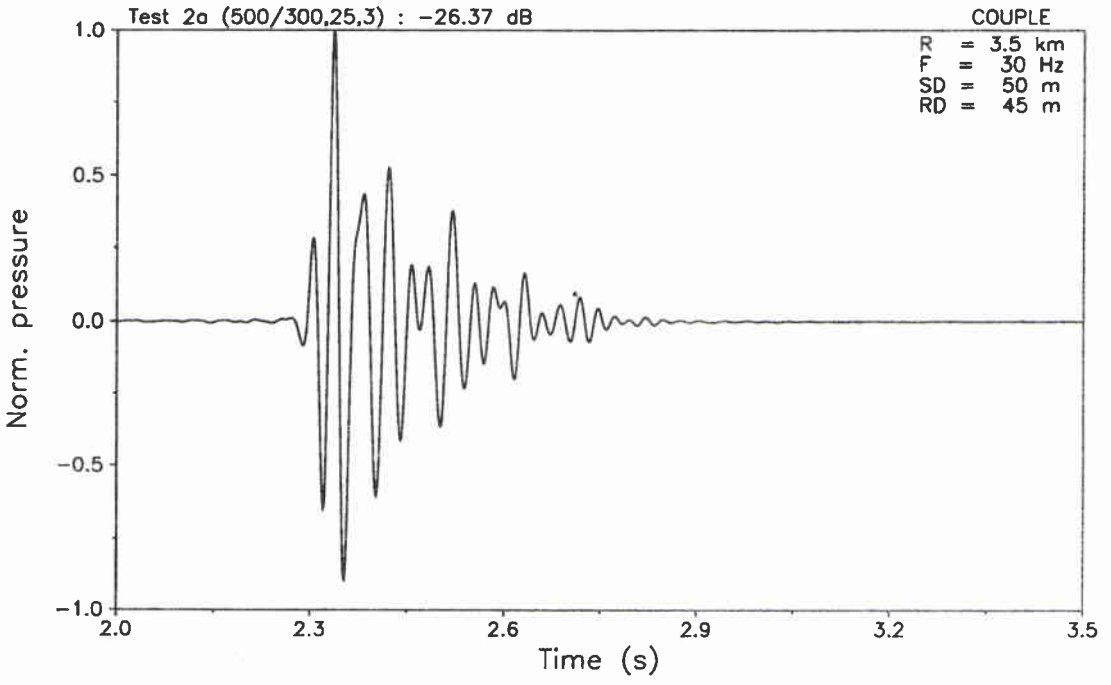

Figure B19 Case 2a: COUPLE solution for the forward scattered signal at range 3.5 km.

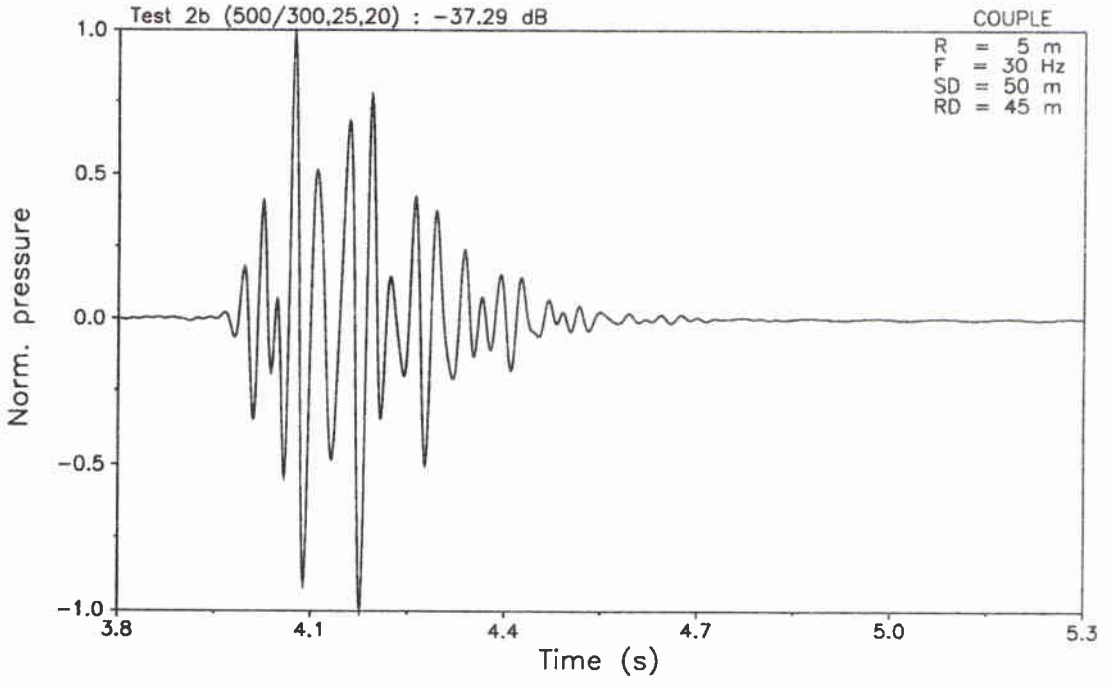

Figure B20 Case 2b: COUPLE solution for the backscattered signal at range 5 m.

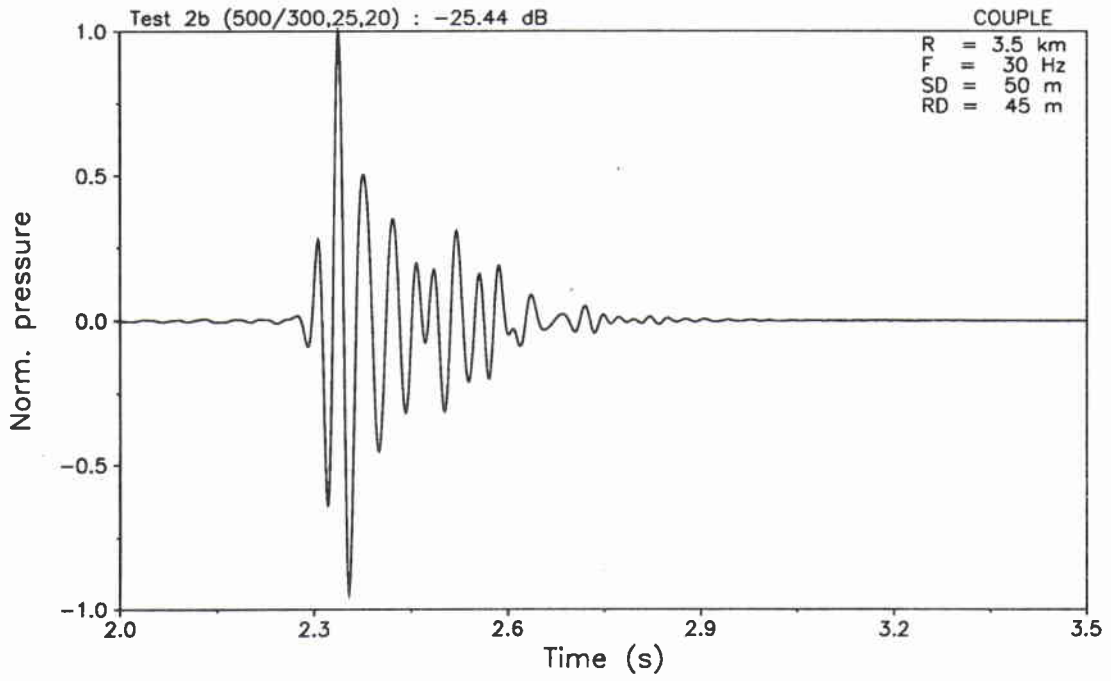

Figure B21 Case 2b: COUPLE solution for the forward scattered signal at range 3.5 km.

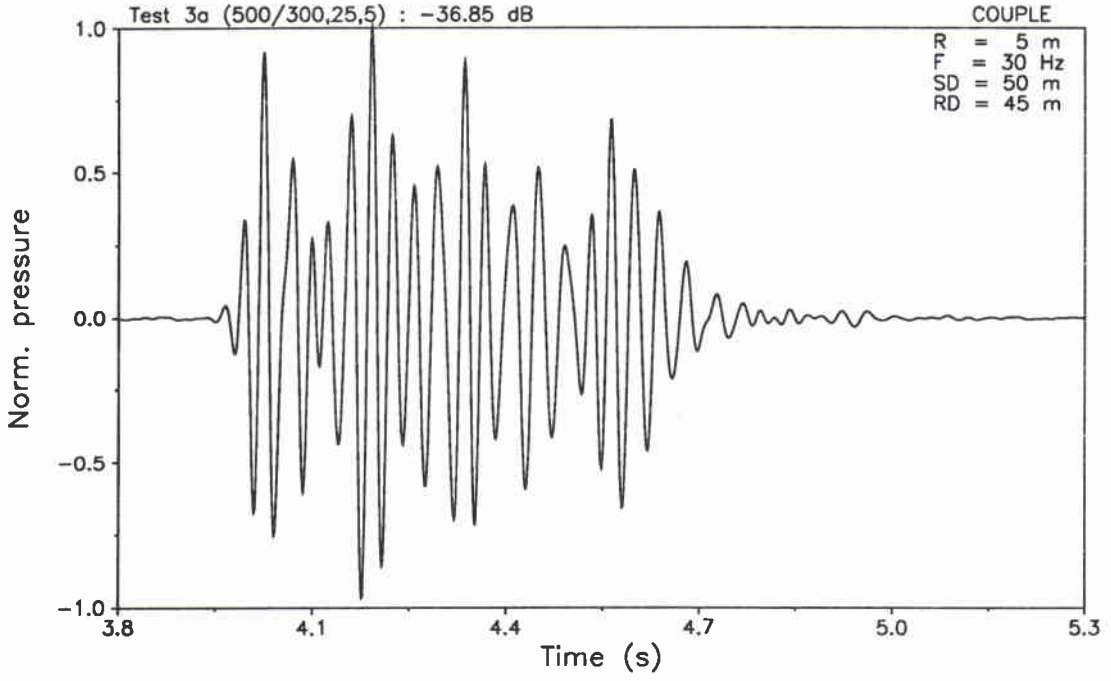

Figure B22 Case 3a: COUPLE solution for the backscattered signal at range 5 m.

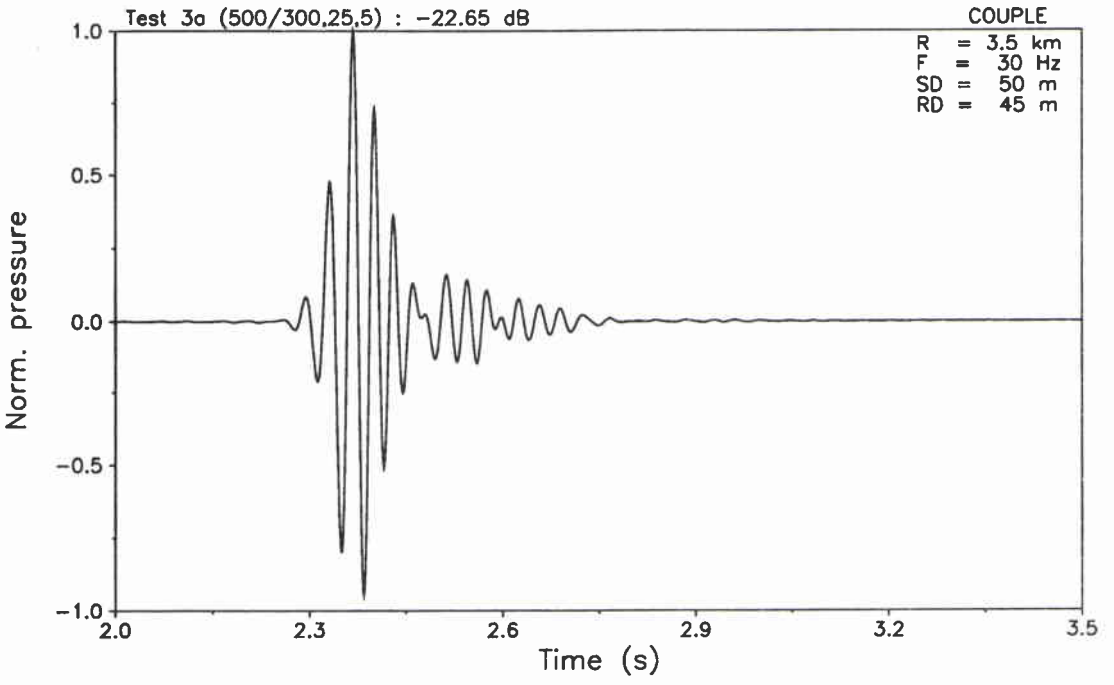

Figure B23 Case 3a: COUPLE solution for the forward scattered signal at range 3.5 km.

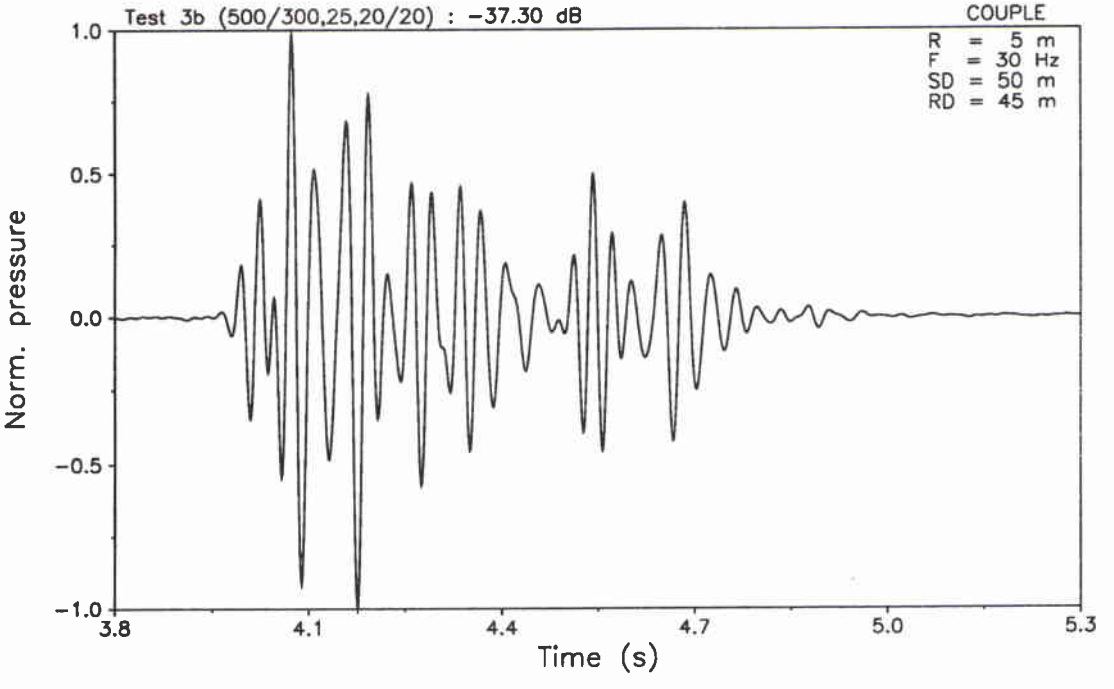

Figure B24 Case 3b: COUPLE solution for the backscattered signal at range 5 m.

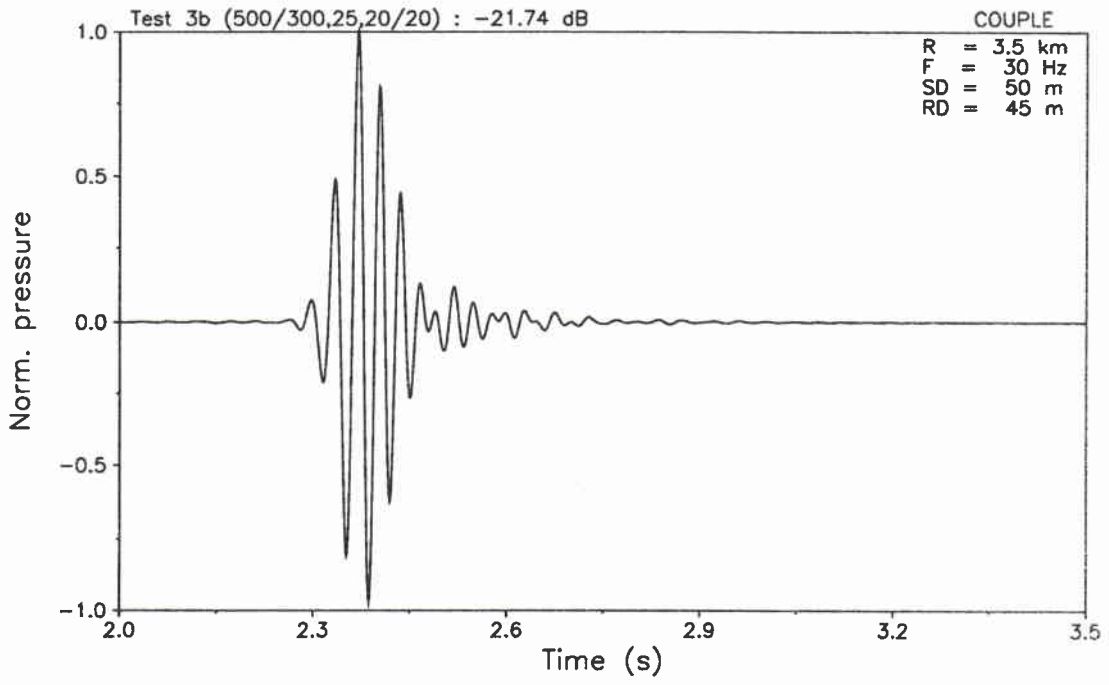

Figure B25 Case 3b: COUPLE solution for the forward scattered signal at range 3.5 km.

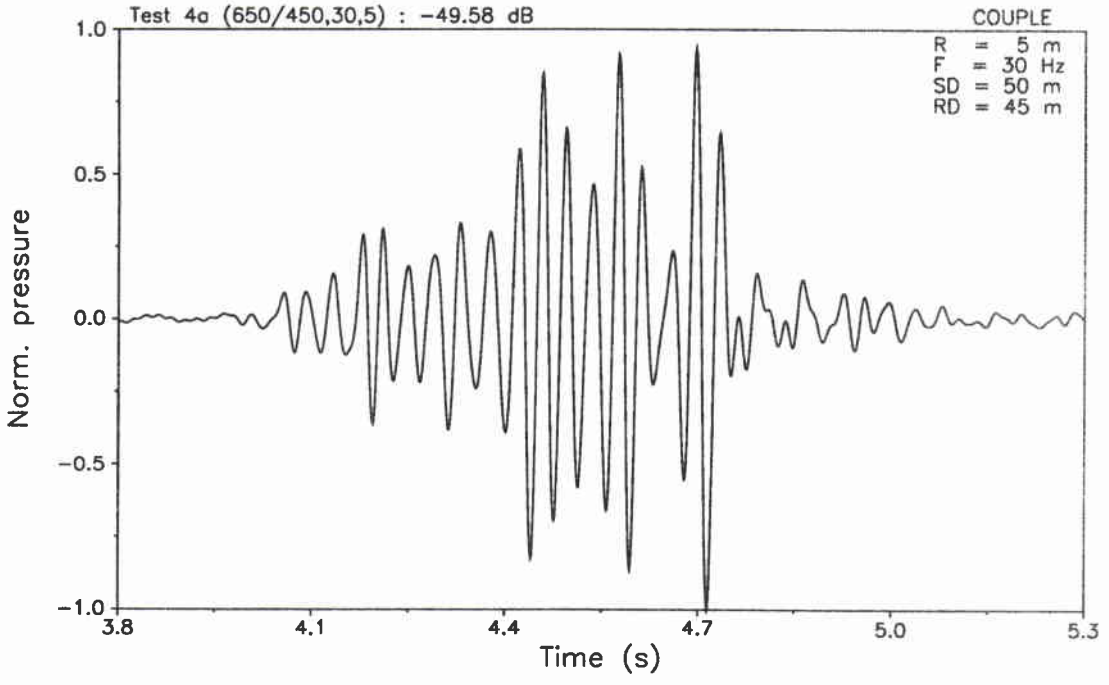

Figure B26 Case 4a: COUPLE solution for the backscattered signal at range 5 m.

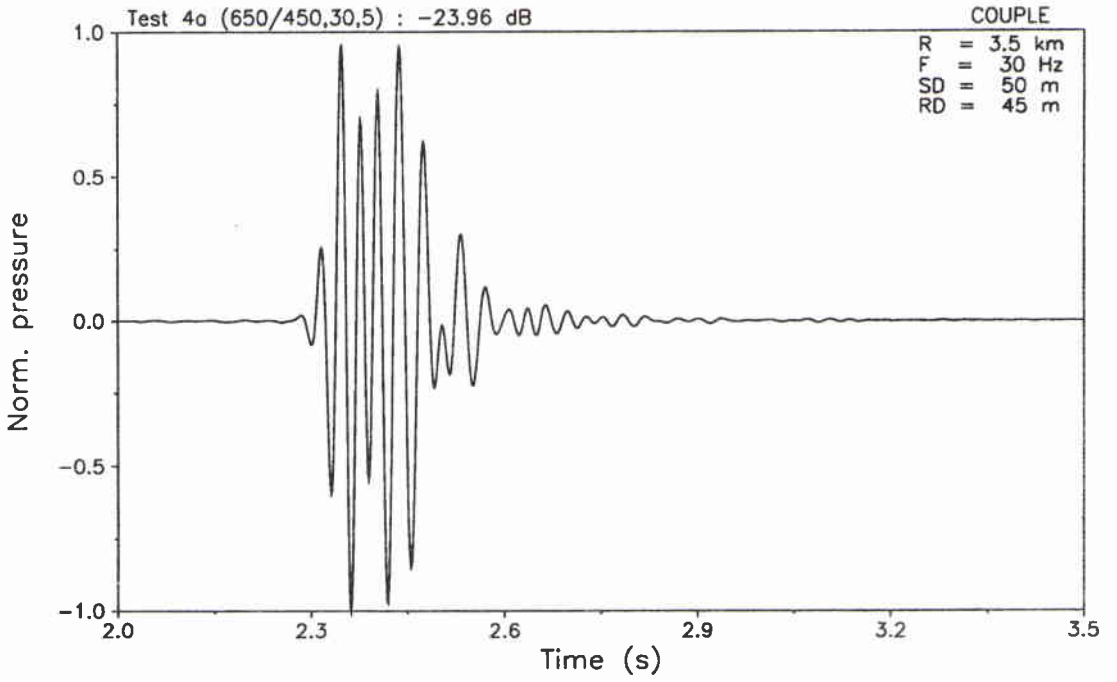

Figure B27 Case 4a: COUPLE solution for the forward scattered signal at range 3.5 km.

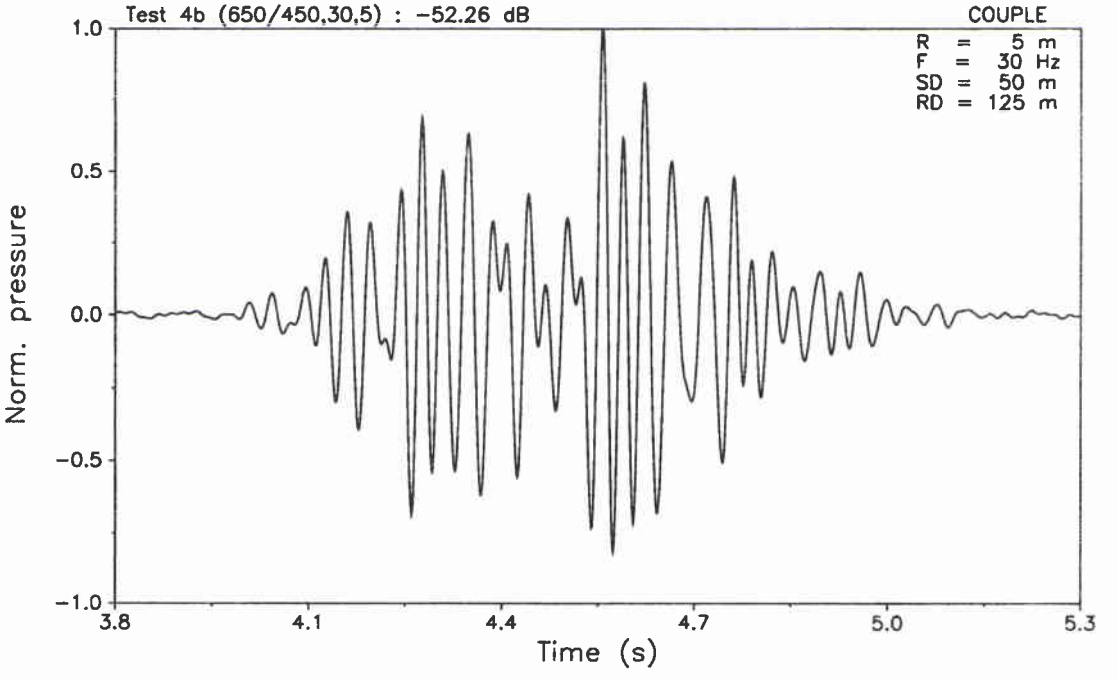

Figure B28 Case 4b: COUPLE solution for the backscattered signal at range 5 m.

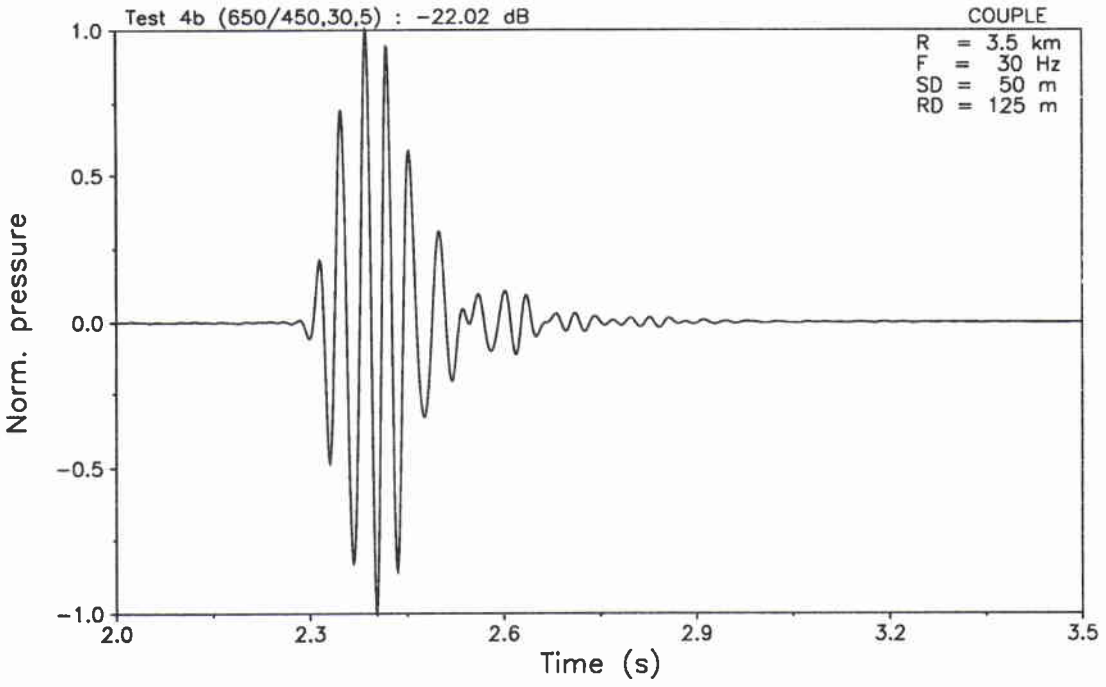

Figure B29 Case 4b: COUPLE solution for the forward scattered signal at range 3.5 km.

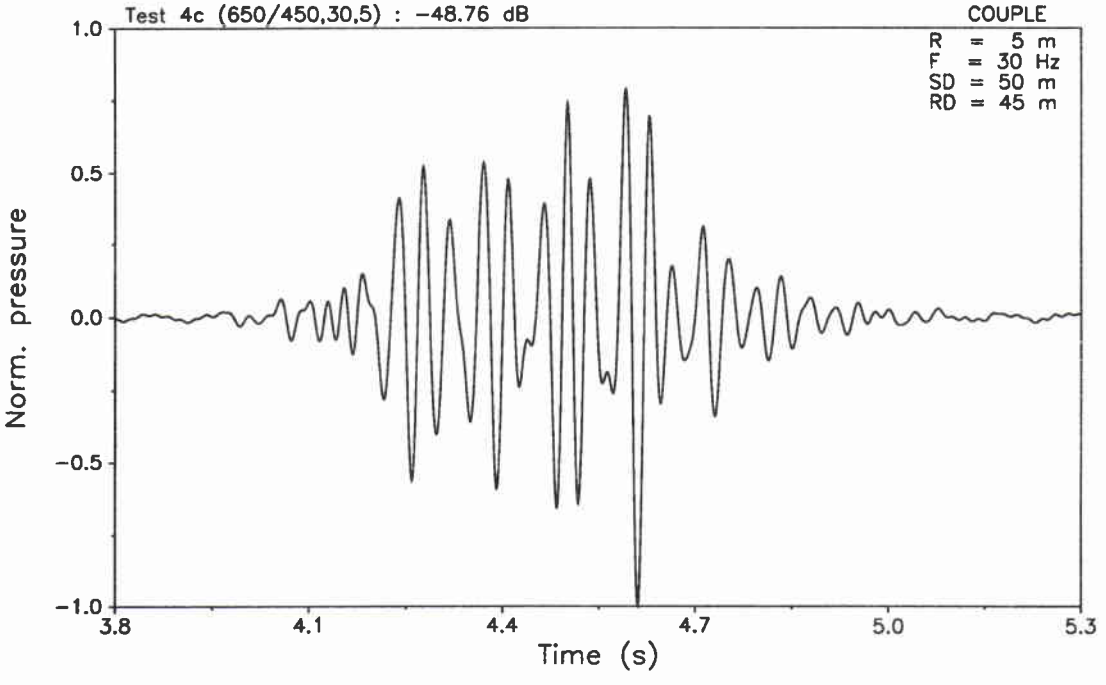

Figure B30 Case 4c: COUPLE solution for the backscattered signal at range 5 m.

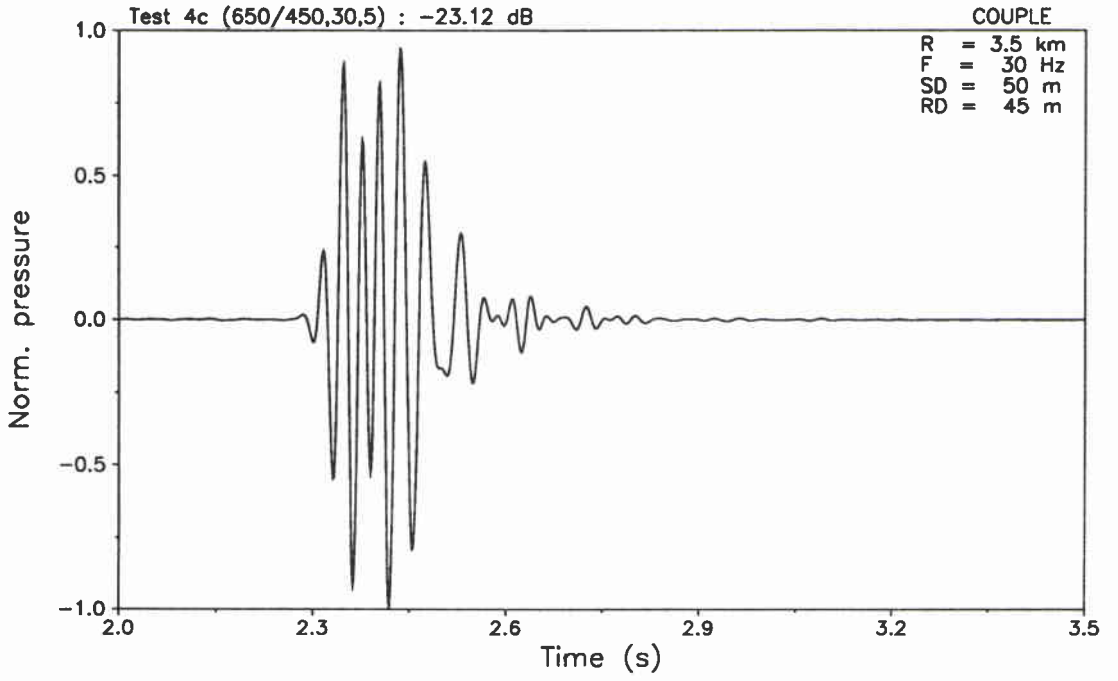

Figure B31 Case 4c: COUPLE solution for the forward scattered signal at range 3.5 km.

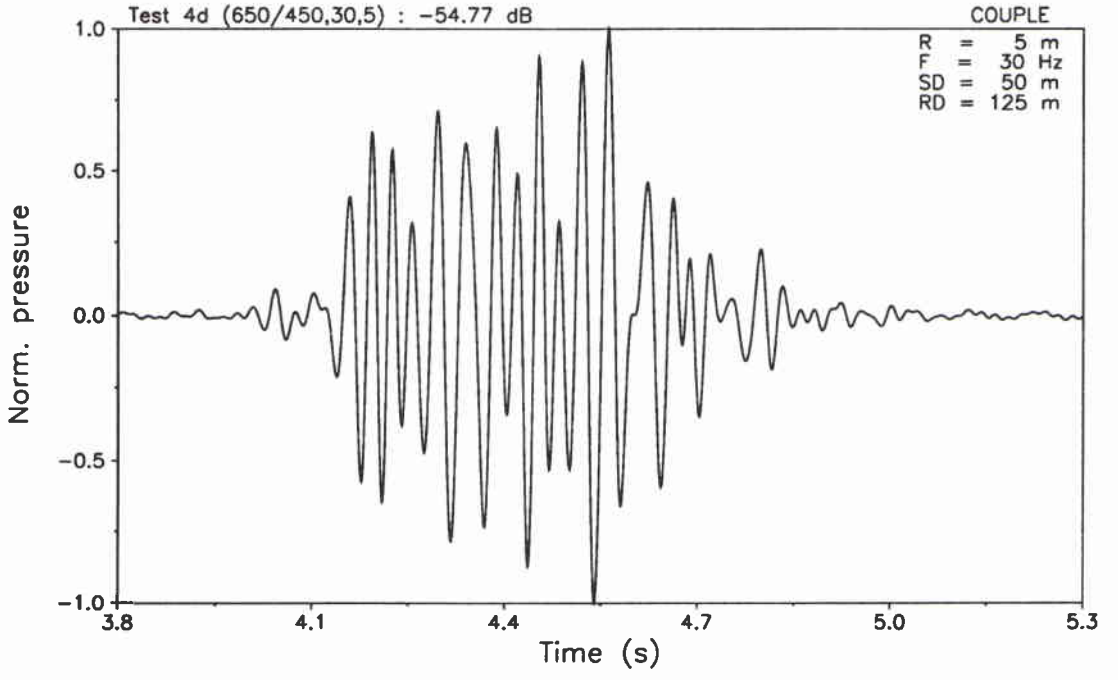

Figure B32 Case 4d: COUPLE solution for the backscattered signal at range 5 m.

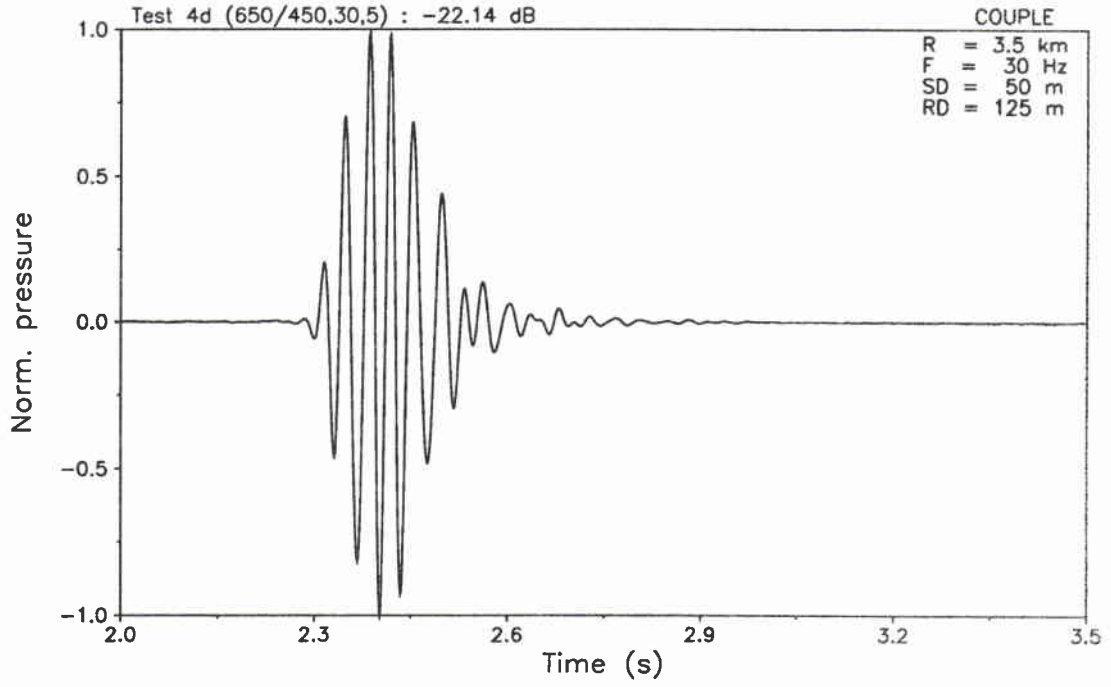

Figure B33 Case 4d: COUPLE solution for the forward scattered signal at range 3.5 km.

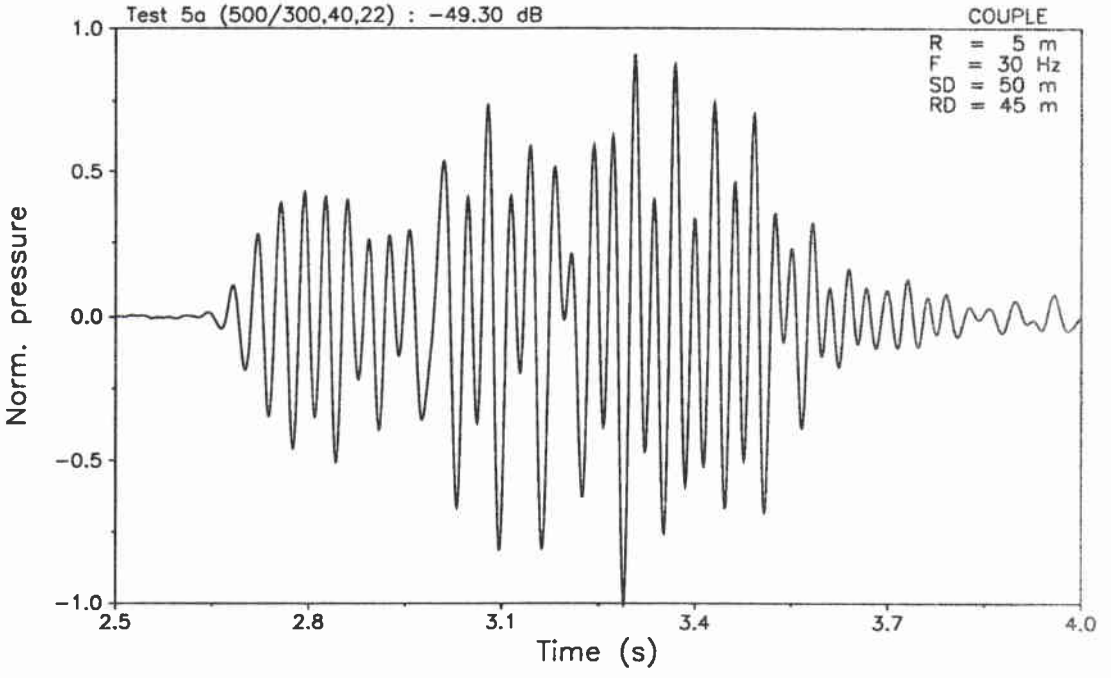

Figure B34 Case 5a: COUPLE solution for the backscattered signal at range 5 m.

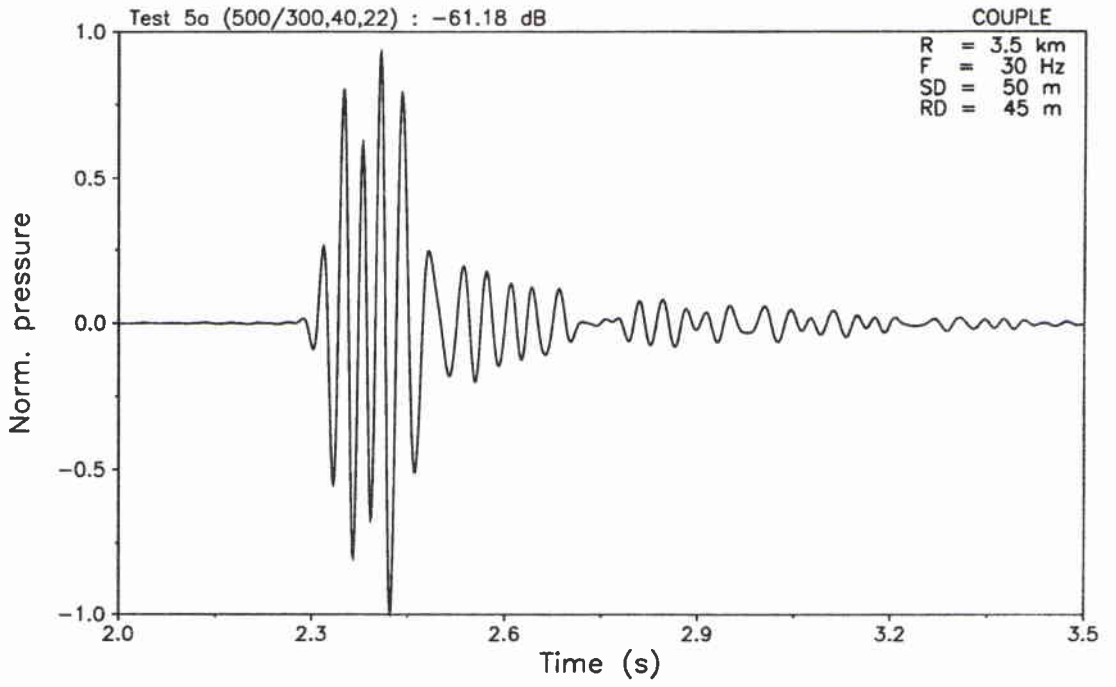

Figure B35 Case 5a: COUPLE solution for the forward scattered signal at range 3.5 km.

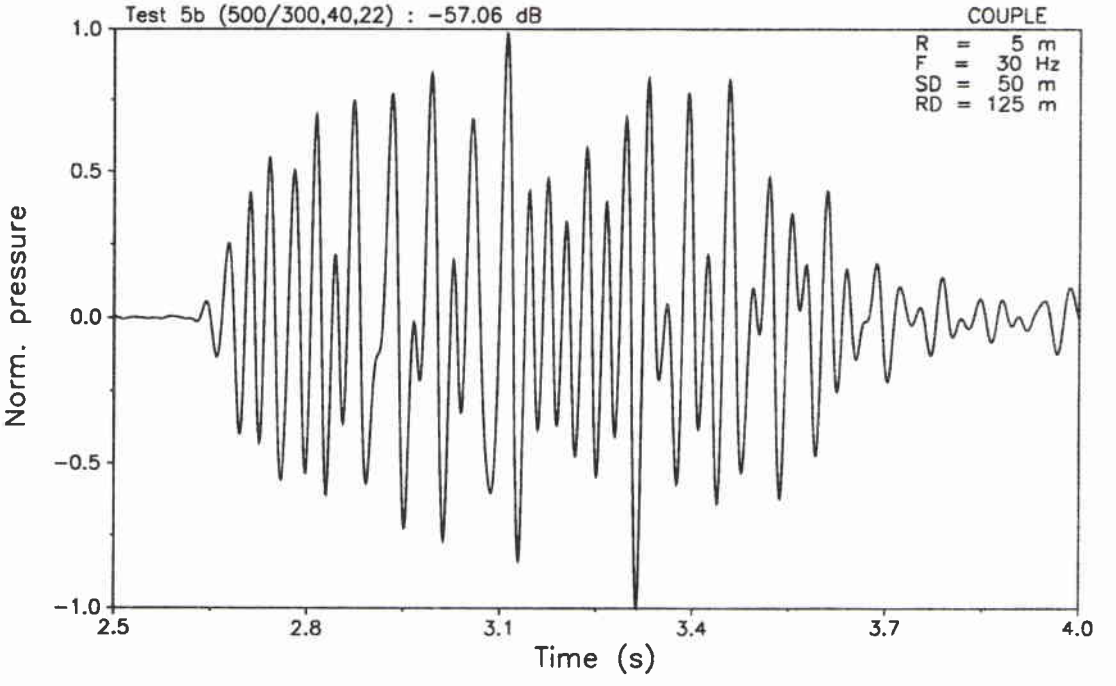

Figure B36 Case 5b: COUPLE solution for the backscattered signal at range 5 m.

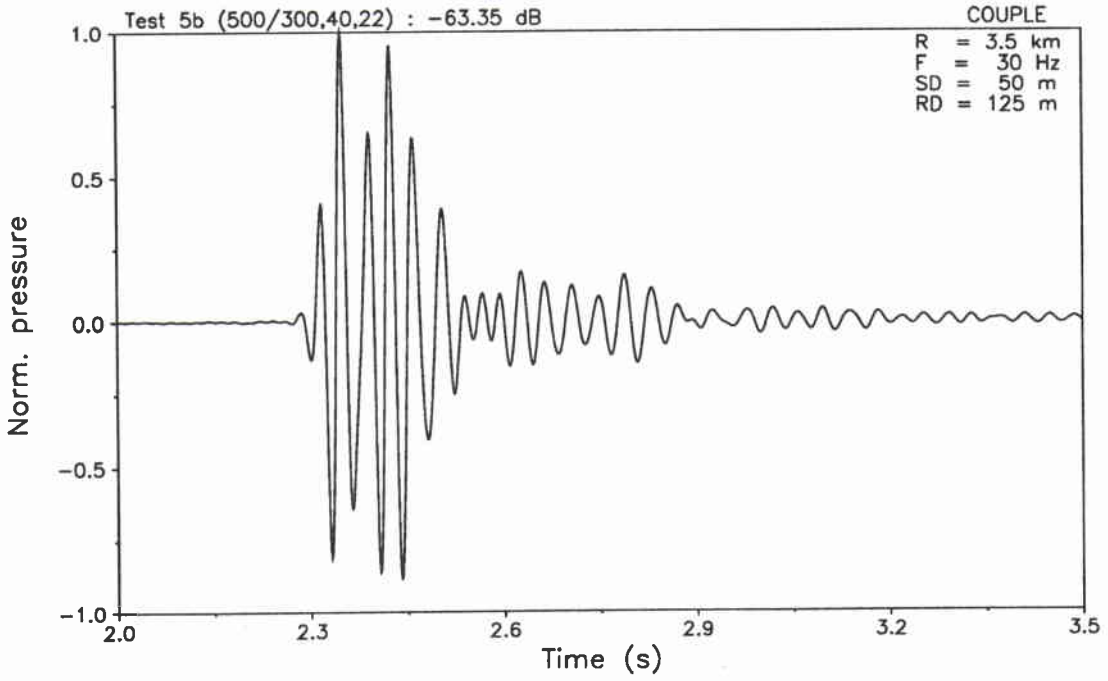

Figure B37 Case 5b: COUPLE solution for the forward scattered signal at range 3.5 km.

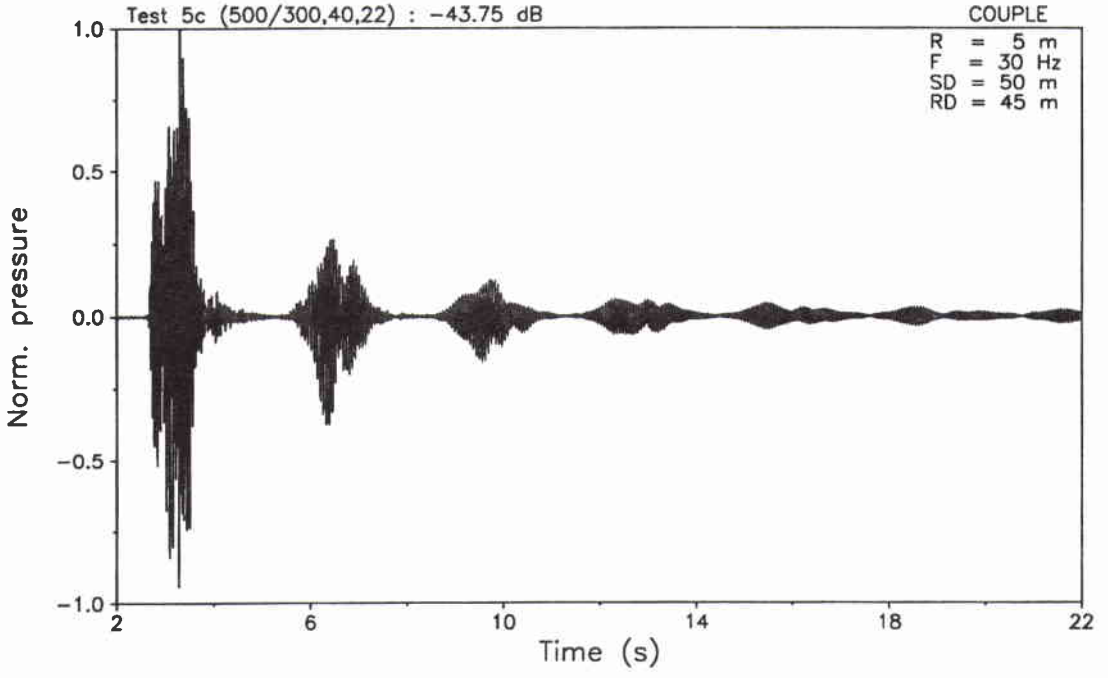

Figure B38 Case 5c: COUPLE solution for the backscattered signal at range 5 m.

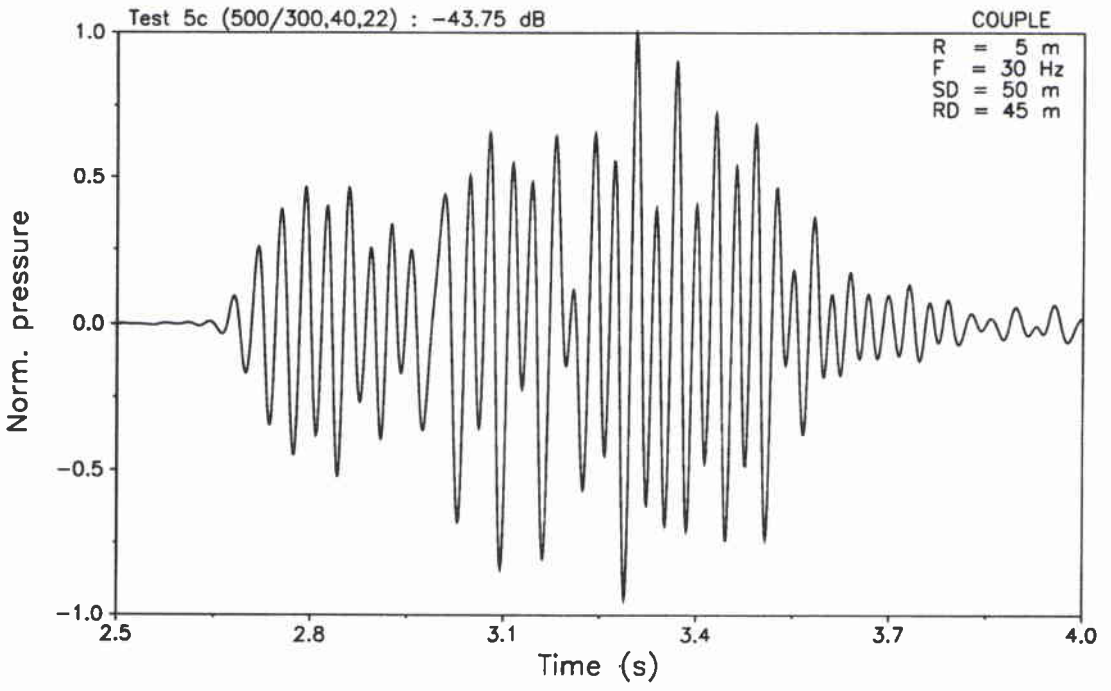

Figure B39 Case 5c: COUPLE solution for the backscattered signal at range 5 m on an extended time scale.

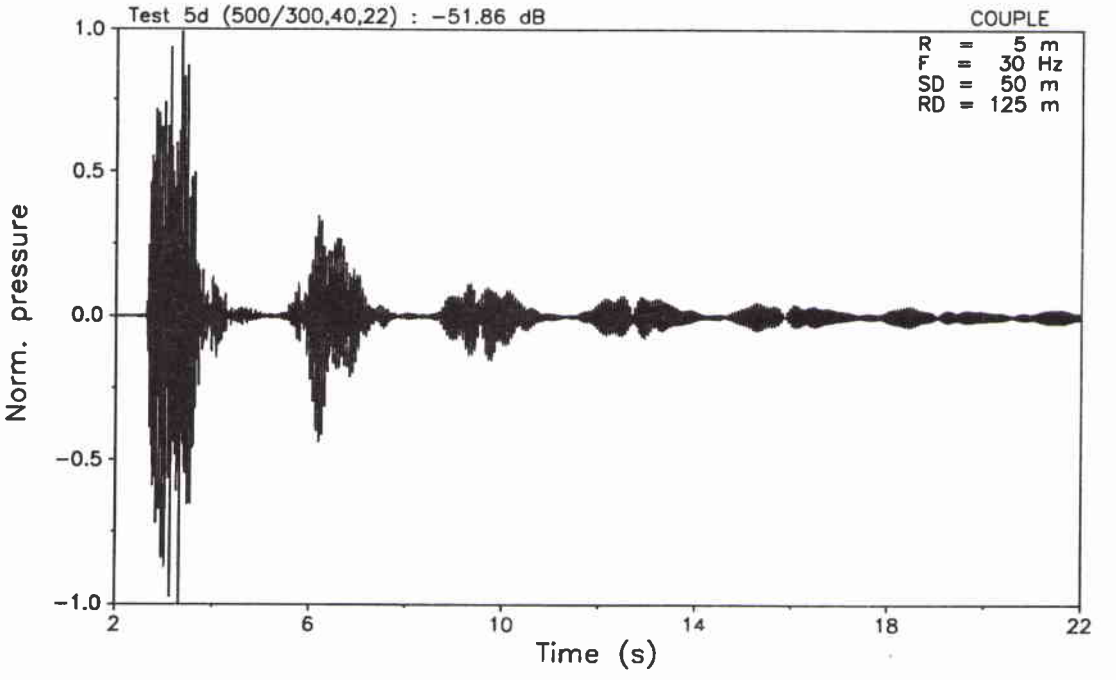

Figure B40 Case 5d: COUPLE solution for the backscattered signal at range 5 m.

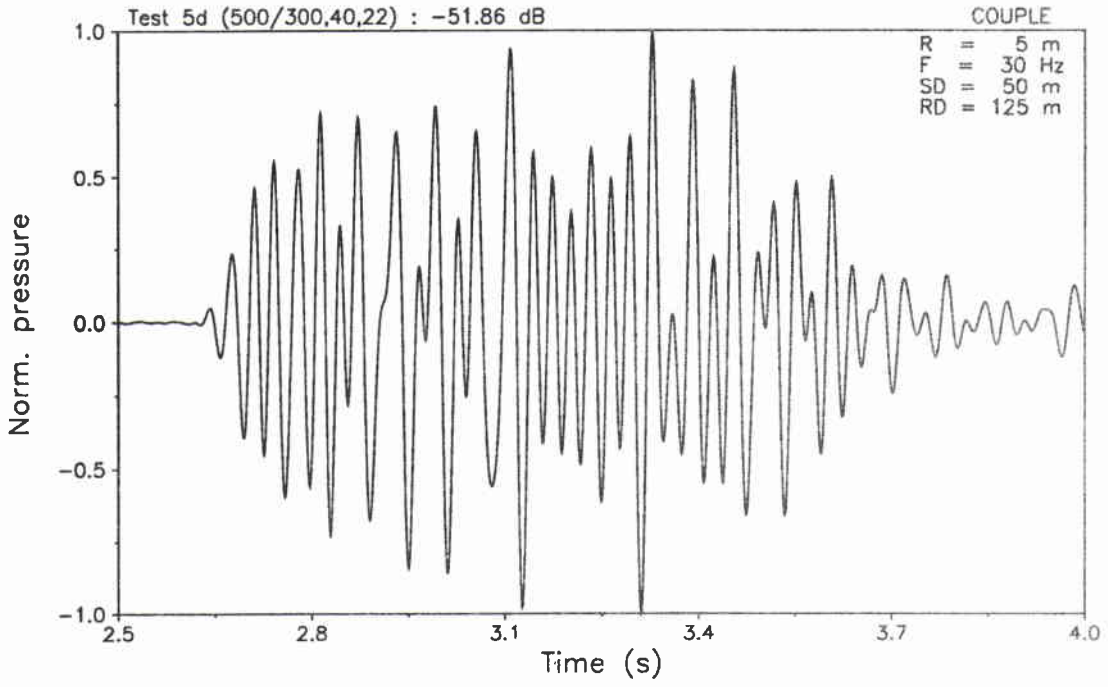

Figure B41 Case 5d: COUPLE solution for the backscattered signal at range 5 m on an extended time scale.

Security Classification		Project No.
NATO UNCLASSIFIED		19
Document Serial No.	**Date of Issue**	**Total Pages**
SM-290	July 1995	64 pp.

Author(s)

F.B. Jensen, C.M. Ferla and P. Gerstoft

Title

Benchmarking scattering in ocean waveguides

Abstract

Accurate numerical solutions are presented for benchmark problems associated with forward scattering from a rough sea surface and with backscattering from obstacles on the seafloor in a shallow-water waveguide. Computational aspects are discussed and both CW (transmission loss at 30 Hz) and broadband (10–50 Hz) time-series solutions are given.

Keywords

numerical modeling, propagation loss, pulse modeling, reverberation, scattering

Issuing Organization

North Atlantic Treaty Organization
SACLANT Undersea Research Centre
Viale San Bartolomeo 400, 19138 La Spezia, Italy

[From N. America: SACLANTCEN CMR-426 (New York) APO AE 09613]

tel: +39-187-540.111
fax: +39-187-524.600

e-mail: library@saclantc.nato.int

Initial Distribution for SM-290

SCNR for SACLANTCEN	
SCNR Belgium	1
SCNR Canada	1
SCNR Denmark	1
SCNR Germany	1
SCNR Greece	1
SCNR Italy	1
SCNR Netherlands	1
SCNR Norway	1
SCNR Portugal	1
SCNR Spain	1
SCNR Turkey	1
SCNR UK	1
SCNR US	2
French Delegate	1
SECGEN Rep. SCNR	1
NAMILCOM Rep. SCNR	1

National Liaison Officers	
NLO Belgium	1
NLO Canada	1
NLO Denmark	1
NLO Germany	1
NLO Italy	1
NLO Netherlands	1
NLO UK	3
NLO US	4

Total external distribution	30
SACLANTCEN Library	20
Total number of copies	50